A molecular mechanism by which amyloid-β induces inactivation of CREB in Alzheimer's Disease

Running title: Jacob induces CREB shut-off in AD

Authors

Katarzyna M. Grochowska[1,2]†, Rahul Kaushik[1,3]†, Guilherme M. Gomes[1,6]†, Rajeev Raman[1]†, Julia Bär[1], Gonca Bayraktar[1], Sebastian Samer[1], Irene Reyes-Resina[1], Christina Spilker[1], Marcel S. Woo[4], Arthur Bikbaev[5,6], Markus Morawski[7], Manuel A. Friese[4], Steffen Rossner[7], Gemma Navarro Brugal[8], Anna Karpova[1,9*]†, Michael R. Kreutz[1,2,3,9*]

Affiliations

[1] RG Neuroplasticity, Leibniz Institute for Neurobiology, Magdeburg, Germany.
[2] Leibniz Group 'Dendritic Organelles and Synaptic Function', Center for Molecular Neurobiology (ZMNH), University Medical Center Hamburg-Eppendorf, Hamburg, Germany.
[3] German Center for Neurodegenerative Diseases (DZNE), Magdeburg, Germany.
[4] Institute of Neuroimmunology and Multiple Sclerosis, Center for Molecular Neurobiology (ZMNH), University Medical Center Hamburg-Eppendorf, Hamburg, Germany.
[5] RG Molecular Physiology, Leibniz Institute for Neurobiology, Magdeburg, Germany.
[6] RG Functional Neurobiology, Institute of Developmental Biology and Neurobiology, Johannes Gutenberg University, Mainz, Germany
[7] Molecular Imaging in Neurosciences, Paul Flechsig Institute of Brain Research, Leipzig, Germany.
[8] Centro de Investigación Biomédica en Red Sobre Enfermedades Neurodegenerativas and Department of Biochemistry and Molecular Biology, Faculty of Biology, University of Barcelona, Barcelona, Spain.
[9] Center for Behavioral Brain Sciences, Otto von Guericke University, Magdeburg, Germany.

† These authors contributed equally to this work.
* E-mail address: michael.kreutz@zmnh.uni-hamburg.de; akarpova@lin-magdeburg.de

Abstract

Disruption of transcriptional activity of cAMP–responsive element-binding protein (CREB), a master regulator of cell survival and plasticity-related gene expression, is a hallmark of Alzheimer's disease (AD). CREB shut-off results in early synaptic dysfunction, contributes to AD pathology and eventually neuronal cell death and is elicited by amyloid-β (Aβ)-induced activation of extrasynaptic N-methyl-D-aspartate-receptors (NMDAR). In previous work we found that the protein messenger Jacob encodes and transduces the synaptic or extrasynaptic origin of NMDAR signals to the nucleus. In response to cell survival and plasticity-related synaptic NMDAR stimulation macromolecular transport of Jacob from synapse-to-nucleus docks the MAP-kinase ERK to the CREB complex which results in sustained CREB phosphorylation. Following disease-related activation of extrasynaptic NMDAR by Aβ Jacob associates with protein phosphatase-1γ (PP1γ) and induces dephosphorylation and transcriptional inactivation of CREB. Binding of the adaptor protein LIM domain only 4 (LMO4) distinguishes extrasynaptic from synaptic NMDAR signaling and determines the affinity for the association with PP1γ. This mechanism contributes to transcriptional inactivation of CREB in the context of early synaptic dysfunction and cell loss in AD. Accordingly, Jacob protein knockdown attenuates Aβ-induced CREB shut-off and Jacob gene knockout is neuroprotective in a transgenic mouse model of AD. Collectively the data suggest that long-distance protein transport from NMDAR to the nucleus is part of early AD pathology and that Jacob docks a signalosome to CREB that is instrumental for CREB shut-off.

Key words: NMDA-receptor, Alzheimer's disease, CREB, cell death, Jacob

Introduction

NMDAR are heteromeric glutamate-gated ion channels implicated in synaptic plasticity, learning and memory but also in neurodegeneration and excitotoxicity [2,16,30]. A prevailing hypothesis suggests that the opposing functions of NMDAR can be attributed to their subunit composition and subcellular localization [2]. In particular activation of GluN2B-containing NMDAR at extrasynaptic sites has been implicated in brain disease states including AD [2,24,25,7]. Signaling downstream of synaptic and extrasynaptic NMDAR is tightly and antagonistically coupled to the activity of the transcription factor CREB. Activation of synaptic NMDAR activates CREB through sustained phosphorylation of a crucial serine at position 133 and thereby promotes the expression of plasticity-related genes [16]. Several studies have shown that gene expression programs triggered by CREB following activation of synaptic NMDAR are critically involved in learning and memory processes [3,9]. Conversely, predominant activation of extrasynaptic NMDAR leads to sustained dephosphorylation of CREB (CREB shut-off), rendering CREB transcriptionally inactive [17]. Loss of CREB-dependent gene expression after extrasynaptic NMDAR activation precedes cell death and neurodegeneration [16] and Aβ-mediated CREB shut-off apparently plays a role in early synaptic dysfunction driving cognitive impairment in AD [35,12,40,43,5]. The underlying mechanisms, as well as their relevance for neurodegeneration are currently unknown.

In previous work, we could show that the synapto-nuclear messenger Jacob (encoded by the *Nsmf* gene), following long-distance transport and nuclear import, transduces the synaptic and extrasynaptic origin of GluN2B-NMDAR signals to the nucleus [11,21,29]. Activation of synaptic NMDARs leads to phosphorylation of Jacob at serine 180 via MAP-kinase ERK1/2, which is followed by trafficking along microtubules of a pJacob/pERK1/2 signalosome to neuronal nuclei [21]. Binding of the intermediate filament α-internexin protects pJacob and pERK against dephosphorylation during transport [21]. This signalosome promotes CREB phosphorylation at serine 133 and hence CREB-dependent gene expression. On the contrary,

activation of extrasynaptic NMDAR by exogenous Aβ application leads to prominent translocation of non-phosphorylated Jacob and induces CREB shut-off followed by stripping of synaptic contacts, simplification of dendritic arborization and cell death [13,15,33]. The data suggest that Jacob operates as a mobile hub that docks NMDAR-derived signalosomes to nuclear target sites [11,21,25,29]. However, the molecular mechanisms behind the Janus-faced regulation of CREB by Jacob are still elusive. In the present study, we addressed two fundamental questions. We first investigated the coupling of extrasynaptic NMDAR signaling to CREB and deciphered the molecular mechanisms of Jacob-induced CREB shut-off. Next, we assessed the physiological significance of this mechanism for AD pathology.

Materials and Methods

Additional information is provided in Supplementary Materials.

Animals

Animals were maintained in the animal facility of the Leibniz Institute for Neurobiology, Magdeburg. Jacob/*Nsmf* knockout animals were characterized before [38]. The TBA2.1 mice [1] were a kind gift from ProBiodrug. To generate double transgenic animals (TBA2.1, -/-) Jacob/*Nsmf* heterozygous mice were crossed with heterozygous TBA2.1 mice. All lines had a C57BL/6 background. Animal experiments were carried out in accordance with the European Communities Council Directive (2010/63/EU) and approved by local authorities of Sachsen-Anhalt/Germany (reference number 42502-2-1264 LIN and 42502-2-1284 UNIMD).

Human brain tissue

The temporal cortex (area 22) biospecimens (Table S1) were provided by the former Brain Banking Centre Leipzig of the German Brain-Net, operated by the Paul Flechsig Institute of

Brain Research (Leipzig University). The diagnosis and staging of Alzheimer's disease cases was based on the presence of neurofibrillary tangles [8] and neuritic plaques in the hippocampal formation and neocortical areas as outlined by the Consortium to establish a registry for Alzheimer's disease (CERAD; [27]) and met the criteria of the National Institute on Aging on the likelihood of dementia (The National Institute on Aging, 1997). For the study of human biospecimens, the informed consent forms and autopsies were approved (GZ 01GI9999-01GI0299).

cDNA constructs, shRNA, recombinant proteins and antibodies

See Table S2.

Interaction studies

Yeast-Two-Hybrid screening for Jacob interaction partners [18], pull-down assays [21] and heterologous co-immunoprecipitation [21] were performed as described previously. The phospho-dependent association of overexpressed nuclear Jacob was assessed by heterologous co-immunoprecipitation from HEK293T cells pre-treated with 20nM staurosporine for 3h.

Fluorescence resonance energy transfer (FRET) and sequential resonance energy transfer (SRET) assays

For FRET experiments, HEK293T cells were transiently co-transfected with different combinations of two genes of interest (Table S2) tagged with donor (GFP) or acceptor (tagRFP), with constant concentration of cDNA of donor and increasing concentration of acceptor. FRET was performed as described previously [10]. For SRET measurements, transfected cells were resuspended in Hank´s balanced salt solution (HBSS) supplemented with 10 mM glucose (Sigma-Aldrich). Triple-transfected (CREB-Rluc:Jacob-GFP:LMO4-tagRFP) cell suspension was used to perform the three measurements. (i) The LMO4-tagRFP

expression level was assessed by the tagRFP fluorescence intensity. (ii) The CREB-Rluc expression level was estimated by CREB-Rluc luminescence determined 10min after addition of coelenterazine-H (5µM). (iii) For SRET, the cells were incubated with 5µM of DeepBlueC (Molecular Probes). The measurements were done with Mithras LB940 (Berthold Technologies) equipped with the detection filters at 400nm and 590nm. Net SRET was defined as [(long-wavelength emission)/(short-wavelength emission)]-Cf, where Cf corresponds to [(long-wavelength emission)/(short-wavelength emission)] for cells expressing CREB-Rluc:Jacob-GFP:LMO4-Myc.

Recombinant protein production

GST-, MBP- and his-SUMO- tagged recombinant proteins were produced and purified as described previously [11,21].

Preparation of protein extracts from human brain

Human brain samples or murine CA1 were homogenized in a buffer containing 0.32M sucrose, 5mM HEPES, protease inhibitors (Sigma) and phosphatase inhibitors (Roche), in a 1g/10ml ratio. The homogenates were centrifuged at 1000g for 10min at 4ºC. The pellets were used for immunoblotting. The band intensities were quantified with Fiji/ImageJ [36].

Neuronal nuclei isolation and flow cytometry

Nuclei were isolated from the protein extracts with the Nuclei Isolation Kit (Sigma Aldrich, cat. no. NUC101) according to the manufacturer's protocol. Nuclei were fixed with ice-cold methanol for 10 min. We used 0.5% Triton for permeabilization and 10% normal donkey's serum for blocking followed by 1h RT incubation with respective primary and, subsequently, secondary antibodies (see Table S2) and counterstained with Hoechst33342 (1:500,

ThermoFisher, Cat.:# H3570). The samples were measured with the BD LSR II flow cytometer (BD Biosciences) and analysed with FlowJo (LLC).

RNA extraction, reverse transcription and quantitative real-time PCR (qPCR)

Hippocamapl homogenization, RNA extraction and cDNA preparation was described previously [38]. *Bdnf exon IV* and *β-actin* (reference gene) cDNA were amplified using the iScript RT-PCR iQ SYBR Green Supermix (BIORAD, Cat.:# 170882) in a qPCR detection system (LightCycler LC480, Roche). The sequences are indicated in Table S2. The relative expression levels were analyzed using the 2-ΔΔCt method with the normalization relative to *β-actin*.

Luciferase assay

Stably transfected HEK293T cell line expressing luciferase under the CRE promoter (vector pGL4.29[luc2P/CRE/Hygro], Promega) transfected for 24h and lysed with the lysis buffer (25mM Tris-phosphate, 2mM DTT, 2mM 1,2-diaminocyclohexane-N,N,N´,N´-tetraacetic acid, 10% glycerol, 1% TX-100, pH 7.8). The luciferase activity was measured with the Dual-Luciferase Reporter Assay System (Promega) on a (FLUOstar Omega, BMG Labtech).

Aβ-oligomer production

Aβ oligomers (Anaspec) were prepared as described previously [15].

Preparation of hippocampal and cortical cultures, transfection and stimulation

Hippocampal and cortical cultures were prepared from Wistar rat embryos (E18) as described in [11]. Hippocampal neuronal cultures were transfected with plasmid cDNAs using Lipofectamine2000 (Thermo Fisher Scientific) following the manufacturer's instructions. For LMO4 knockdown cells were expressing shRNA for 5 days; for Jacob knockdown 4 days. For

CREB shut-off experiments hippocampal neurons were transfected at DIV15 and fixed after 24h. For the experiment with okadaic acid (OA, Tocris) cells were treated for 20min with 2µM OA 1 day post transfection. The target sequences for LMO4 and NLS-Jacob knockdown [38] as well as scrambled controls are indicated in Table S2. For Aβ-induced CREB shut-off experiments transfected neurons were treated for 40min with 500nM $A\beta_{1-42}$ or $A\beta_{3(pE)-42}$.

Cultured murine hippocampal slices (OHSC), stimulation, and immunocytochemistry

OHSC were prepared according to previously published protocols [15]. Slices were prepared from P7-P9 C57/B6J or Jacob/*Nsmf* knockout mice. For Aβ-induced CREB shut-off 7 DIV OHSC were treated with 1µM $A\beta_{1-42}$ oligomeric solution for 1h, fixed for 1h at RT in 4% paraformaldehyde (PFA)/4% sucrose. After fixation the slices were washed, permeabilized with 0.4% TX-100 and treated with 50 mM NH_4Cl for 30min. Subsequently, the samples were blocked for 1h in RT in 10% normal goat serum (NGS) in PBS. Next, the slices were incubated for 72h with primary antibody. Then slices were incubated with secondary antibody for 24h. Following counterstaining with 4',6-diamidino-2-phenylindole (DAPI; Vectashield/Biozol), the samples were mounted in Mowiol 4-88 (Merck Chemicals).

Animal perfusion, immunohistochemistry, and image analysis

Animals were anesthetized with ketamine (Medistar)-Rompun (Bayer), perfused with 0.9% NaCl, and fixed with 4% PFA in PBS for 4min. The brains were post-fixed in 4% PFA in PBS overnight and subsequently left for soaking in 0.5M sucrose, followed by 1M sucrose. The brains were snap-frozen and cut into 35 µm thick coronal cryosections (Leica CM3050S, Leica-Microsystems). The sections were blocked in a buffer (0.3% TX-100, 10% NGS in PBS) for 30min at RT, and incubated with primary antibodies diluted in the blocking solution, overnight at 4ºC. Secondary antibodies were applied for 2h at RT. Sections were counterstained with DAPI and mounted in Mowiol 4-88. For the detection of Aβ, the heat-

based antigen retrieval method was used. Following permeabilization, brain sections were immersed into 10µM sodium citrate solution (Fluka, pH=9) for 30min at 80°C. Imaging of nuclear pCREB/CREB immunoreactivities in cryosections was performed using a Leica TCS SP5 system (Leica-Microsystems). Images were acquired sequentially with a HCX ApoL20x/1.0 water objective, optical zoom 4. Sections were imaged with constant laser/detector settings along the z-axis with 400nm step in a 512x512 pixel format.

All quantifications were done within the distal CA1 of hippocampus. Fiji/ImageJ [36] was used to calculate maximum intensity projection from five optical sections for each channel. CREB and pCREB immunoreactivity of every single nucleus in a 100µm stretch was measured in arbitrary units of pixel intensity. ROIs were defined based on NeuN and DAPI. The neuronal loss was quantified based on NeuN staining (the number of neurons/CA1 length). For the quantification of microglia and astrocytes the number of cells based on overlaid DAPI and Iba-1 or GFAP signal was quantified within the rectangular ROI. Aβ plaques were counted in the region where the neuronal loss was quantified.

Immunocytochemistry

Dissociated cultures were fixed with 4% PFA/4% sucrose solution for 10min at RT, washed with PBS and subsequently permeabilized with 0.2% TX-100 in PBS for 10min. Then, cells were incubated for 1h in blocking solution (2% glycine, 0.2% gelatin, 2% BSA, and 50mM NH_4Cl (pH 7.4)) and primary antibodies were applied overnight at 4ºC. Next, the coverslips were incubated with secondary antibodies diluted 1:500. Coverslips were mounted with Mowiol 4-88. For detection of Jacob-CREB and Jacob-LMO4 co-localization in STED imaging, a heat-based antigen retrieval protocol was used.

Quantification of nuclear staining intensity

For quantification of nuclear staining intensity somatic regions were sequentially scanned using the 63x objective (Leica) in both: Leica TCS SP8-STED and Leica TCS SP5 systems. Image format was set either to 1024x1024 or 512x512 with optical zoom 4. Average intensity images from three optical sections (Z-step300nm) were generated and intensity measurements were performed within the ROIs defined by DAPI. The values were normalized to the mean intensity of the control group. Unprocessed images were analysed using Fiji/ImageJ [36] software. For visualization of the quantified channel a fire look up table (LUT) was used. For some representative images linear contrast-enhancement (histogram normalization) was applied equally for all groups. The figures were created with Adobe Illustrator software.

Statistical analysis

Merged group data were represented as mean ±S.E.M. Cumulative frequency distribution of nuclei staining intensities, graphs and statistical analysis were made with GraphPad Prism (GraphPad Software). To choose the appropriate statistical analysis, a normality test (Shapiro-Wilk test) was performed. The statistical tests used for analysis and the N number are described in the figure legends. For qPCR data Ct values were subjected to both Dixon's and Grubb's outlier test.

Results

Jacob is a direct binding partner of CREB and LMO4

To decipher the molecular mechanism underlying Jacob-induced CREB shut-off we first asked whether both proteins might be in one complex. Super-resolution stimulated emission depletion (STED) imaging revealed a tight association of CREB with Jacob in the nucleus of cultured hippocampal neurons (Fig. S1a, b). We could co-immunoprecipitate endogenous CREB from HEK293T cells following heterologous expression of Jacob (Fig. S1c) and a direct

interaction was confirmed by pull-down of bacterially expressed proteins (Fig. 1a) where we observed an association of both N-terminal (117-172 aa) and C-terminal (262-532 aa) regions of Jacob to the bZIP domain of CREB (Fig. S1d-f). In support of these data we found significant *in vivo* FRET efficiency when we co-expressed either full-length or the N-terminal half of Jacob and a C-terminal fragment of CREB (Fig. 1b-e). Of note, the N-terminal fragment of Jacob yielded significantly stronger fluorescence resonance energy transfer (FRET) signals than the C-terminal fragment (Fig. 1b-e).

In a yeast two-hybrid (YTH) screen performed with the N-terminus of Jacob as bait we identified LMO4 as a binding partner (Fig. S2a). A region encompassing aa 117-228 of Jacob interacts with the LIM1 domain of LMO4 (Fig. S2a). Pull-down assays revealed direct binding (Fig. 1f, Fig. S2b, c). Both proteins are in close proximity to each other in neuronal nuclei (Fig. S2d, e) and the LIM1 domain co-localizes with cytosolic Jacob clusters following heterologous expression (Fig. S2f). The association was further confirmed by heterologous co-immunoprecipitation with tag-specific antibodies (Fig. S2g) and a direct interaction was corroborated by *in vivo* FRET analysis (Fig. 1g-i). Heterologous co-immunoprecipitation of Jacob fragments with the LIM1 domain suggests that the binding interfaces for LMO4 and CREB do not overlap (Fig. 1j). LMO4 is a transcriptional co-activator of CREB [22] and we therefore wondered whether the Jacob-LMO4 interaction has a role in Jacob-induced CREB shut-off. The binding interface for LMO4 frequently contains hydrophobic amino acids like leucine (L) or valine (V) [20]. Jacob contains such a leucine-rich stretch and when we introduced corresponding point mutations (L175A-V176A, Fig. 1k) the mutant protein exhibited clearly weaker binding (Fig. 1k-m). We have previously shown that nuclear overexpression without stimulation of synaptic NMDAR leads to dephosphorylation of CREB [11]. Interestingly, nuclear accumulation of the LMO4 binding mutant of Jacob did not induce CREB shut-off (Fig. 1n-p), indicating that the association with LMO4 is instrumental for Jacob-induced dephosphorylation of CREB.

Jacob competes with CREB for LMO4 binding

Evidence for a direct interaction came from *in vivo* FRET assays where we found that the LIM1 domain, which is also the binding interface for Jacob (Fig. 1i, j, Fig. S2a-c), interacts with a C-terminal fragment of CREB (Fig. 2a-c). Pull-down revealed that LMO4 directly binds to this region but not like Jacob to the isolated bZIP domain of CREB (Fig. 2d-f, Fig. S2c). Heterologous expression of LMO4 increases CRE-driven luciferase activity (Fig. 2g). Interestingly, shRNA knockdown of LMO4 (Fig. S2h-j) in neurons reduces nuclear pCREB immunofluorescence (Fig. 2h, i) but not total CREB levels (Fig. 2j, k). Thus, the direct interaction with LMO4 promotes phosphorylation of Ser133 and thereby CREB transcriptional activity. Direct binding of LMO4 to CREB and Jacob raises the question whether all three proteins can assemble in a trimeric complex or whether they compete for the same binding interface. Sequential resonance energy transfer (SRET) *in vivo* indeed revealed the existence of a triple complex (Fig. 2l, m). Jacob harbors a binding interface for the interaction with CREB and LMO4 at the N-terminus (Fig. 1) whereas LMO4 can only associate through the first LIM1 domain either to Jacob or to CREB (Fig. 1, 2). Subsequent competition pull-down experiments confirmed competitive binding between the N-terminus of Jacob and CREB with LMO4 when GST-LMO4 was coupled to the beads and increasing amounts of the N-terminal fragment of Jacob were added in the presence of CREB (Fig. 2n-p). In summary, the LIM1 domain of LMO4 mediates either the association with CREB or Jacob and Jacob is capable to displace LMO4 from the CREB complex, a mechanism that should facilitate CREB shut-off.

PP1γ binds to nuclear Jacob and is involved in Jacob-induced CREB shut-off

Previous work has shown the involvement of PP1 in NMDA-induced CREB shut-off [34]. Jacob harbors several PP1 binding motifs, both proteins co-localize following heterologous expression (Fig. S3a) and tagged Jacob co-immunoprecipitates with endogenous

PP1γ (Fig. S3b). Pull-down experiments established a direct interaction (Fig. 3a, Fig. S3c) and heterologous co-immunoprecipitation experiments revealed two binding interfaces (Fig. 3b). We next addressed whether the association with PP1γ is crucial for Jacob-induced CREB shut-off. To this end we expressed a phosphodeficient mutant of Jacob in the nucleus of hippocampal primary neurons [21] and incubated cultures with the PP1γ inhibitor okadaic acid (OA). Interestingly, we found that treatment with OA indeed prevented Jacob-induced CREB shut-off (Fig. 3c, d).

Phosphorylation of Jacob at serine 180 is induced by activation of synaptic NMDAR, whereas nuclear import of the non-phosphorylated protein is related to extrasynaptic NMDAR activation [21]. Accordingly, in a CRE-luciferase activity assay the expression of wild-type but not phosphodeficient Jacob caused increased activity (Fig. 3e, Fig. S3d). These data indicate that Jacob associates with CREB regardless of Ser180 phosphorylation, however, association of a phosphodeficient mutant of Jacob is significantly stronger with LMO4 than the corresponding phosphomimetic protein (Fig. 3f, g, Fig. S3e). Phosphomimetic Jacob, unlike the non-phosphorylated protein, did not displace CREB from LMO4 bound to the beads (Fig. 3h, i, Fig. 2n-p). To further test the notion that LMO4 binds to non-phosphorylated Jacob more efficiently we applied the protein kinase inhibitor staurosporine and performed heterologous co-immunoprecipitation experiments (Fig. 3j, k). We indeed found a stronger association of non-phosphorylated Jacob to LMO4 (Fig. 3j, k) and concomitantly a stronger association of Ser180 phosphorylated Jacob to CREB (Fig. 3j, k). Since Jacob directly interacts with PP1γ (Fig. 3a) we performed a pull-down assay where we found that the association between both proteins became much stronger in the presence of LMO4 (Fig. 3l, m, Fig. S3e, f). Thus, non-phosphorylated Jacob, entering the nucleus following activation of extrasynaptic NMDAR, will displace LMO4 from the CREB complex and the association with LMO4 will enhance binding to PP1γ.

Jacob protein knockdown reduces NMDA-induced CREB shut-off

We next asked for functional consequences of the differential phosphorylation of Jacob for neuronal activity. To this end we infected neurons plated on microelectrode arrays (MEAs) with a virus expressing phosphomimetic or phosphodeficient Jacob (Fig. S3g-i). We then monitored neuronal firing and observed that expression of phosphodeficient Jacob - which induces CREB shut-off - strongly suppressed spiking and bursting activity in the neuronal network established on the array whereas expression of phosphomimetic Jacob was associated with marked enhancement of neuronal activity (Fig. S3g-i). The displacement of LMO4 from CREB and a subsequent enhanced association with PP1γ provides a conceivable molecular mechanism for CREB shut-off. We therefore next investigated the role of Jacob in NMDA-induced CREB shut-off in mature hippocampal neurons. pCREB levels were monitored after bath application of NMDA for different periods of time (Fig. S4a). In accord with previous work [11], protein knockdown of nuclear Jacob rescued NMDA-induced CREB shut-off in hippocampal primary neurons (Fig. S4a-c). Surprisingly, however, neither oxygen-glucose deprivation (OGD) nor NMDA-induced cell death differed in organotypic hippocampal slice cultures from Jacob/*Nsmf* -/- animals and wild-type littermates (Fig. S5).

Jacob/*Nsmf* gene knockout protects against Aβ toxicity

Since Jacob/*Nsmf* gene deletion does not confer neuroprotection in ischemia or acute NMDA-induced excitotoxicity in organotypic slices we wondered whether CREB shut-off might gain more pathophysiological relevance in slowly progressing disease states like AD. Jacob plays a role in Aβ-induced CREB shut-off that is elicited by activation of extrasynaptic GluN2B containing NMDAR [13,15,33]. In the brain of AD patients, Aβ oligomers can be found in various, post-translationally modified forms [23], out of which the N-terminally truncated, pyroglutamylated $A\beta_{3(pE)-42}$ species are very prominent [19]. $A\beta_{1-42}$ and $A\beta_{3(pE)-42}$

induced CREB shut-off cause the impairment of synaptic function with subsequent synapse loss via pathways that converge on nuclear import of nonphosphorylated Jacob [15]. shRNA knockdown of Jacob in hippocampal neurons prevented CREB shut-off induced by treatment of cultures with 500 nM $A\beta_{1-42}$ or $A\beta_{3(pE)-42}$ (Fig. 4a, b). Similar results were obtained with organotypic hippocampal slices from Jacob/*Nsmf* knockout mice or wild-type littermates treated with 1 μM of $A\beta_{1-42}$ oligomers (Fig. 4c-f). Basal pCREB nuclear immunofluorescence levels were not different between both genotypes, however, neurons from Jacob/*Nsmf* knockout mice, unlike the wild-type, did not display $A\beta_{1-42}$—induced CREB shut-off (Fig. 4c, d). Total CREB levels remained unchanged (Fig. 4e, f).

Jacob/*Nsmf* gene knockout ameliorates neuronal loss in transgenic AD mice

The lack of Aβ-induced CREB shut-off in Jacob/*Nsmf* knockout mice should confer neuroprotection in AD. The CA1 subfield of the hippocampus is one of the earliest areas affected in AD, with pronounced neuronal loss and a decreased number of synaptic contacts [28]. To study the contribution of Jacob we chose a mouse model with clear Aβ-induced neurodegeneration. TBA2.1 mice express $A\beta_{3(pE)-42}$ and display severe CA1 neuronal loss, amyloidosis, LTP impairment, and neuroinflammation [1].

Western blot analysis of protein extracts from TBA2.1 mice revealed unchanged Jacob protein levels (Fig. 5a, d) but significantly decreased pJacob levels and a reduced pJacob/Jacob ratio (Fig. 5b-d). In accordance with reports from other AD transgenic mouse lines [43,5], we found that TBA2.1 mice exhibit significantly reduced nuclear pCREB levels (Fig. 5e-g). To study whether the loss of Jacob expression in neurons confers neuroprotection we next crossed homozygous TBA2.1 and Jacob/*Nsmf* -/- mice. Interestingly, the double transgenic animals (TBA2.1 x Jacob/*Nsmf* -/-) did not display evidence for CREB shut-off (Fig. 5e-g). Although we observed in all three genotypes (TBA2.1, Jacob/*Nsmf* -/-, and double transgenic) slightly decreased nuclear pan-CREB levels as compared to wild-type mice (Fig. 5h-j), the lack of

CREB shut-off in Jacob/*Nsmf* knockout and double transgenic animals makes a strong case for a key role of Jacob in CREB shut-off at an early stage of AD. Moreover, cell loss in the dorsal CA1 region of TBA2.1 was by far less pronounced in double transgenic mice (on average 23%) (Fig. 5k). BDNF is a neurotrophic factor whose expression is modulated by Jacob in a CREB-dependent manner [38]. Interestingly, the degree of neuronal loss correlates with hippocampal *BdnfIV* mRNA levels, which are statistically significant decreased only in TBA2.1 mice, but not in Jacob/*Nsmf* -/- and double transgenic animals (Fig. 5l).

Jacob/*Nsmf* gene deletion does not influence the number of astrocytes (Fig. S6a, b) and activated microglia (Fig. S6a, c), indicating comparable neuroinflammation in TBA2.1 mice and double transgenic animals (Fig. S6a-c). Moreover, amyloid load, evidenced by the number of Aβ-positive puncta, (Fig. S6d, e) was not affected by removal of the Jacob/*Nsmf* gene.

CREB shut-off and reduced pJacob levels in brains of AD patients

Collectively these results indicate that indirect effects of neuroinflammation or amyloid deposition cannot account for the neuroprotection conferred by Jacob/*Nsmf* gene deletion. It is, thus, likely that indeed Jacob-induced CREB shut-off plays a role in AD pathology. We therefore decided to examine the levels of pJacob and Jacob in nuclear-enriched protein extracts from post mortem tissue of the temporal cortex from Alzheimer's disease patients. Similar to TBA2.1 mice, immunoblots from a nuclear enriched fraction obtained from the temporal cortex of AD patients and corresponding controls did not reveal a significant reduction in total Jacob levels (Fig. 6a, b; Fig. S7a, b). However, the levels of pJacob were significantly decreased by roughly 40% (Fig. 6c, d; Fig. S7a, c), indicating that nuclear import of Jacob following activation of synaptic NMDAR is diminished probably at the expense of activation of extrasynaptic NMDAR. Expectedly we observed significant neuronal loss in AD patients as evidenced by NeuN-immunoblotting (Fig. 6e, f). Jacob is, unlike CREB, exclusively expressed in neurons [26]. We next compared the phosphorylation status of nuclear Jacob normalized to

total protein levels and corrected these values for NeuN content to adjust for neuronal cell loss (Fig. 6g). With this measure we also observed a clear reduction of the pJacob/Jacob ratio (Fig. 6g). This in turn was correlated with the degree of CREB shut-off that we had to determine following FACS sorting of NeuN-positive nuclei (Fig. 6h-j, Fig. S7d), given that CREB is expressed in both, astrocytes and neurons.

Discussion

AD patients display reduced pCREB levels in the prefrontal cortex [4], hippocampus [31] and the temporal cortex as shown in the present work. A central role of CREB shut-off in early AD pathology has been suggested in numerous studies [39,43,12]. The molecular mechanisms underlying CREB shut-off, however, remained elusive. Here we revealed a molecular mechanism implying Aβ-induced extrasynaptic NMDAR activation and nuclear import of Jacob for the induction of CREB shut-off. We provide evidence that Jacob directly associates with the bZIP domain of CREB and we further could show that binding of an adaptor protein determines whether Jacob associates with the CREB phosphatase PP1γ or ERK1/2, which in turn is decisive whether Jacob induces inactivation of CREB or enhanced CREB-dependent gene transcription (Fig. 6k).

Of note, Jacob-induced CREB shut-off is not relevant for acute excitotoxic cell death. This might be explained by the fact that lack of CREB-dependent pro-survival and plasticity-relevant gene expression is not causative for instantaneous cell death like for instance breakdown of the mitochondrial membrane potential [17]. Jacob-induced CREB shut-off kicks in when extrasynaptic NMDAR activation by agents like oligomeric Aβ is continuous and results in cellular degeneration induced by altered gene transcription. Finally, it should be emphasized that no other molecular mechanism for long-lasting transcriptional inactivation of CREB in neurons has been described yet and it is tempting to speculate that this mechanism will

also contribute to early synaptic dysfunction and later on cell death in other neurodegenerative diseases.

A mechanism for CREB shut-off in AD

Since Jacob is a regulator of long-lasting CREB shut-off it is likely that it will contribute to the pathology of neurodegenerative diseases like AD. In the present study we were able to decipher the underlying mechanism in very much detail. We observed that LMO4 directly binds to CREB. LMO4 is a transcriptional co-activator of CREB [22] and our data suggest that LMO4 will hinder dephosphorylation of Ser133, stabilize the CREB dimer and thereby act as a transcriptional enhancer. Jacob displaces LMO4 from the CREB complex (Fig. 6k), and this might further contribute to long-lasting CREB dephosphorylation. Thus, enhanced binding of Jacob to PP1γ and displacement of LMO4, renders the association with LMO4 a key event for Jacob-induced CREB shut-off. PP1γ phosphatase activity is regulated by a large and growing number of targeting subunits, as well as by a smaller number of inhibitor proteins that interact with PP1γ in a mutually exclusive manner [6]. It is therefore an open question whether Jacob might also displace an inhibitor from PP1γ and thereby regulate its activity or whether it serves exclusively as a targeting subunit.

CREB and the Jacob-signalosome in AD: A target for interventions?

The CA1 region of the dorsal hippocampus is among the first to exhibit AD pathology in humans. Moreover, it shows deficits in CREB activation, neuronal complexity, and neuronal network activity in both human patients and mouse AD models [5,43]. Increasing pCREB levels in the CA1 region of Alzheimer's disease mice improves spatial memory, and reverses the deficits in dendritic arborization and neuronal network activity [43]. The results of this rescue closely mirrors those of previous studies in which synaptic pathology was reversed by restoring CREB function by rolipram [14] or its analogue GEBR-7b [37]. Interestingly, the improvement in spatial memory occurred independently of Aβ plaque load and might be related to the extent

of synapse loss, which is a more robust correlate of cognitive impairment in AD patients at an early stage than Aβ or neurofibrillary tangle pathology [4,14,37]. Thus, measures to enhance CREB activity might restore learning and memory through compensatory mechanisms that circumvent Aβ pathology. In previous work we found that one of the earliest phenotypes following nuclear accumulation of non-phosphorylated Jacob is the stripping of synaptic contacts [11,21]. Given that the most promising therapeutic window is before disease onset, right at the beginning of synaptic dysfunction, this is an interesting observation, and Jacob might be an attractive target for interventions to promote plasticity. In fact, interventions are conceivable that will drive the nuclear import of a synaptic Jacob-signalosome to counteract CREB shut-off and improve cognition. For example, rolipram might induce ERK-dependent phosphorylation of Jacob at Ser180 and thereby counteract the deleterious effects of Aβ and activation of extrasynaptic NMDAR.

On the other hand, preventing the formation of Jacob signalosomes related to activation of extrasynaptic GluN2B-containing NMDAR could further minimize the Aβ-induced CREB shut-off. It was shown previously that administration of memantine, a drug that preferentially inhibits extrasynaptic NMDAR [42], alleviates the symptoms in patients with moderate-to-severe disease progression [32]. Memantine rescued synaptic depression by abolishing extrasynaptic NMDAR-induced synaptic impairment [39]. It was also shown to enhance CREB phosphorylation and to restore cognitive function [41]. It is therefore tempting to speculate that the beneficial effects of memantine in AD result at least in part by reduced nuclear translocation of Jacob from extrasynaptic NMDAR.

Collectively the data of the present study suggest that long-distance protein transport from NMDAR to the nucleus is a novel and attractive target for interventions in neurodegenerative diseases.

Acknowledgments

General: The authors gratefully acknowledge the professional technical assistance of M. Marunde, C. Borutzki and S. Hochmuth. We would like to thank Dr. Schilling and Probiodrug for the generous gift of the TBA2.1 mouse line and Dr. Głów for the help with virus production.

Funding: Supported by grants from the Deutsche Forschungsgemeinschaft (DFG) (Kr 1879/9-1/FOR 2419, Kr1879/5-1/6-1/10-1; CRC 779 TPB8; Research Training Group 2413 SynAGE), BMBF 'Energi' FKZ: 01GQ1421B, The EU Joint Programme—Neurodegenerative Disease Research (JPND) project STAD (FKZ: 01ED1613) and Leibniz Foundation SAW 2017 'Neurotranslation' to MRK. People Programme (Marie Curie Actions) of the European Union's Seventh Framework Programme FP7/2007-2013/under REA grant agreement no. [289581], H2020 Priority Excellent Science, Marie Sklodowska-Curie Actions (MSCA) MC-ITN NPlast to KMG, CS, MRK. DFG CRC 779 TPB8 to AK. U.S. Alzheimer's Association, grant Ref. No. AARFD-17-503612 to GNB. DAAD/CAPES scholarship, Alexander-von-Humboldt Foundation Fellowship (1756/14-1) and CBBS NeuroNetwork grant to GMG. GRK1167 scholarship to RK. The authors declare that they have no competing financial interests.

Ethics declarations

The authors report no competing interests.

References

1. Alexandru A, Jagla W, Graubner S, Becker A, Bäuscher C, Kohlmann S, Sedlmeier R, Raber KA, Cynis H, Rönicke R, Reymann KG, Petrasch-Parwez E, Hartlage-Rübsamen M, Waniek A, Rossner S, Schilling S, Osmand AP, Demuth H-U, von Hörsten S (2011) Selective hippocampal neurodegeneration in transgenic mice expressing small amounts of truncated Aβ is induced by pyroglutamate-Aβ formation. The Journal of neuroscience : the official journal of the Society for Neuroscience 31:12790-12801. doi:10.1523/JNEUROSCI.1794-11.2011
2. Bading H (2017) Therapeutic targeting of the pathological triad of extrasynaptic NMDA receptor signaling in neurodegenerations. J Exp Med 214:569-578. doi:10.1084/jem.20161673
3. Barco A, Alarcon JM, Kandel ER (2002) Expression of constitutively active CREB protein facilitates the late phase of long-term potentiation by enhancing synaptic capture. Cell 108:689-703. doi:10.1016/s0092-8674(02)00657-8
4. Bartolotti N, Bennett DA, Lazarov O (2016) Reduced pCREB in Alzheimer's disease prefrontal cortex is reflected in peripheral blood mononuclear cells. Mol Psychiatry 21:1158-1166. doi:10.1038/mp.2016.111
5. Bartolotti N, Segura L, Lazarov O (2016) Diminished CRE-Induced Plasticity is Linked to Memory Deficits in Familial Alzheimer's Disease Mice. J Alzheimers Dis 50:477-489. doi:10.3233/jad-150650
6. Bollen M, Peti W, Ragusa MJ, Beullens M (2010) The extended PP1 toolkit: designed to create specificity. Trends Biochem Sci 35:450-458. doi:10.1016/j.tibs.2010.03.002
7. Bordji K, Becerril-Ortega J, Nicole O, Buisson A (2010) Activation of extrasynaptic, but not synaptic, NMDA receptors modifies amyloid precursor protein expression pattern and increases amyloid-ß production. J Neurosci 30:15927-15942. doi:10.1523/jneurosci.3021-10.2010
8. Braak H, Braak E (1991) Neuropathological stageing of Alzheimer-related changes. Acta neuropathologica 82:239-259. doi:10.1007/bf00308809
9. Carlezon WA, Jr., Duman RS, Nestler EJ (2005) The many faces of CREB. Trends Neurosci 28:436-445. doi:10.1016/j.tins.2005.06.005
10. Carriba P, Navarro G, Ciruela F, Ferre S, Casado V, Agnati L, Cortes A, Mallol J, Fuxe K, Canela EI, Lluis C, Franco R (2008) Detection of heteromerization of more than two proteins by sequential BRET-FRET. Nat Methods 5:727-733. doi:10.1038/nmeth.1229
11. Dieterich DC, Karpova A, Mikhaylova M, Zdobnova I, Konig I, Landwehr M, Kreutz M, Smalla KH, Richter K, Landgraf P, Reissner C, Boeckers TM, Zuschratter W, Spilker C, Seidenbecher CI, Garner CC, Gundelfinger ED, Kreutz MR (2008) Caldendrin-Jacob: a protein liaison that couples NMDA receptor signalling to the nucleus. PLoS Biol 6:e34. doi:10.1371/journal.pbio.0060034
12. Espana J, Valero J, Minano-Molina AJ, Masgrau R, Martin E, Guardia-Laguarta C, Lleo A, Gimenez-Llort L, Rodriguez-Alvarez J, Saura CA (2010) beta-Amyloid disrupts activity-dependent gene transcription required for memory through the CREB coactivator CRTC1. J Neurosci 30:9402-9410. doi:10.1523/jneurosci.2154-10.2010
13. Gomes GM, Dalmolin GD, Bär J, Karpova A, Mello CF, Kreutz MR, Rubin MA (2014) Inhibition of the polyamine system counteracts beta-amyloid peptide-induced memory impairment in mice: involvement of extrasynaptic NMDA receptors. PLoS One 9:e99184. doi:10.1371/journal.pone.0099184
14. Gong B, Vitolo OV, Trinchese F, Liu S, Shelanski M, Arancio O (2004) Persistent improvement in synaptic and cognitive functions in an Alzheimer mouse model after rolipram treatment. J Clin Invest 114:1624-1634. doi:10.1172/jci22831

15. Grochowska KM, Yuanxiang P, Bär J, Raman R, Brugal G, Sahu G, Schweizer M, Bikbaev A, Schilling S, Demuth HU, Kreutz MR (2017) Posttranslational modification impact on the mechanism by which amyloid-beta induces synaptic dysfunction. EMBO Rep 18:962-981. doi:10.15252/embr.201643519
16. Hardingham GE, Bading H (2010) Synaptic versus extrasynaptic NMDA receptor signalling: implications for neurodegenerative disorders. Nat Rev Neurosci 11:682-696. doi:10.1038/nrn2911
17. Hardingham GE, Fukunaga Y, Bading H (2002) Extrasynaptic NMDARs oppose synaptic NMDARs by triggering CREB shut-off and cell death pathways. Nat Neurosci 5:405-414. doi:10.1038/nn835
18. Helmuth M, Altrock W, Böckers TM, Gundelfinger ED, Kreutz MR (2001) An electrotransfection protocol for yeast two-hybrid library screening. Analytical biochemistry 293:149-152. doi:10.1006/abio.2001.5107
19. Jawhar S, Wirths O, Bayer TA (2011) Pyroglutamate amyloid-β (Aβ): a hatchet man in Alzheimer disease. The Journal of biological chemistry 286:38825-38832. doi:10.1074/jbc.R111.288308
20. Joseph S, Kwan AH, Stokes PH, Mackay JP, Cubeddu L, Matthews JM (2014) The structure of an LIM-only protein 4 (LMO4) and Deformed epidermal autoregulatory factor-1 (DEAF1) complex reveals a common mode of binding to LMO4. PloS one 9:e109108-e109108. doi:10.1371/journal.pone.0109108
21. Karpova A, Mikhaylova M, Bera S, Bär J, Reddy PP, Behnisch T, Rankovic V, Spilker C, Bethge P, Sahin J, Kaushik R, Zuschratter W, Kahne T, Naumann M, Gundelfinger ED, Kreutz MR (2013) Encoding and transducing the synaptic or extrasynaptic origin of NMDA receptor signals to the nucleus. Cell 152:1119-1133. doi:10.1016/j.cell.2013.02.002
22. Kashani AH, Qiu Z, Jurata L, Lee SK, Pfaff S, Goebbels S, Nave KA, Ghosh A (2006) Calcium activation of the LMO4 transcription complex and its role in the patterning of thalamocortical connections. J Neurosci 26:8398-8408. doi:10.1523/jneurosci.0618-06.2006
23. Kummer MP, Heneka MT (2014) Truncated and modified amyloid-beta species. Alzheimers Res Ther 6:28. doi:10.1186/alzrt258
24. Malinow R (2012) New developments on the role of NMDA receptors in Alzheimer's disease. Curr Opin Neurobiol 22:559-563. doi:10.1016/j.conb.2011.09.001
25. Marcello E, Di Luca M, Gardoni F (2018) Synapse-to-nucleus communication: from developmental disorders to Alzheimer's disease. Curr Opin Neurobiol 48:160-166. doi:10.1016/j.conb.2017.12.017
26. Mikhaylova M, Karpova A, Bär J, Bethge P, YuanXiang P, Chen Y, Zuschratter W, Behnisch T, Kreutz MR (2014) Cellular distribution of the NMDA-receptor activated synapto-nuclear messenger Jacob in the rat brain. Brain Struct Funct 219:843-860. doi:10.1007/s00429-013-0539-1
27. Mirra SS, Heyman A, McKeel D, Sumi SM, Crain BJ, Brownlee LM, Vogel FS, Hughes JP, van Belle G, Berg L (1991) The Consortium to Establish a Registry for Alzheimer's Disease (CERAD). Part II. Standardization of the neuropathologic assessment of Alzheimer's disease. Neurology 41:479-486. doi:10.1212/wnl.41.4.479
28. Padurariu M, Ciobica A, Mavroudis I, Fotiou D, Baloyannis S (2012) Hippocampal neuronal loss in the CA1 and CA3 areas of Alzheimer's disease patients. Psychiatr Danub 24:152-158
29. Panayotis N, Karpova A, Kreutz MR, Fainzilber M (2015) Macromolecular transport in synapse to nucleus communication. Trends Neurosci 38:108-116. doi:10.1016/j.tins.2014.12.001

30. Parsons MP, Raymond LA (2014) Extrasynaptic NMDA receptor involvement in central nervous system disorders. Neuron 82:279-293. doi:10.1016/j.neuron.2014.03.030
31. Pugazhenthi S, Wang M, Pham S, Sze CI, Eckman CB (2011) Downregulation of CREB expression in Alzheimer's brain and in Abeta-treated rat hippocampal neurons. Mol Neurodegener 6:60. doi:10.1186/1750-1326-6-60
32. Reisberg B, Doody R, Stoffler A, Schmitt F, Ferris S, Mobius HJ (2003) Memantine in moderate-to-severe Alzheimer's disease. N Engl J Med 348:1333-1341. doi:10.1056/NEJMoa013128
33. Rönicke R, Mikhaylova M, Ronicke S, Meinhardt J, Schroder UH, Fandrich M, Reiser G, Kreutz MR, Reymann KG (2011) Early neuronal dysfunction by amyloid beta oligomers depends on activation of NR2B-containing NMDA receptors. Neurobiol Aging 32:2219-2228. doi:10.1016/j.neurobiolaging.2010.01.011
34. Sala C, Rudolph-Correia S, Sheng M (2000) Developmentally regulated NMDA receptor-dependent dephosphorylation of cAMP response element-binding protein (CREB) in hippocampal neurons. J Neurosci 20:3529-3536
35. Saura CA, Valero J (2011) The role of CREB signaling in Alzheimer's disease and other cognitive disorders. Rev Neurosci 22:153-169. doi:10.1515/rns.2011.018
36. Schindelin J, Arganda-Carreras I, Frise E, Kaynig V, Longair M, Pietzsch T, Preibisch S, Rueden C, Saalfeld S, Schmid B, Tinevez J-Y, White DJ, Hartenstein V, Eliceiri K, Tomancak P, Cardona A (2012) Fiji: an open-source platform for biological-image analysis. Nature methods 9:676-682. doi:10.1038/nmeth.2019
37. Sierksma AS, van den Hove DL, Pfau F, Philippens M, Bruno O, Fedele E, Ricciarelli R, Steinbusch HW, Vanmierlo T, Prickaerts J (2014) Improvement of spatial memory function in APPswe/PS1dE9 mice after chronic inhibition of phosphodiesterase type 4D. Neuropharmacology 77:120-130. doi:10.1016/j.neuropharm.2013.09.015
38. Spilker C, Nullmeier S, Grochowska KM, Schumacher A, Butnaru I, Macharadze T, Gomes GM, Yuanxiang P, Bayraktar G, Rodenstein C, Geiseler C, Kolodziej A, Lopez-Rojas J, Montag D, Angenstein F, Bär J, D'Hanis W, Roskoden T, Mikhaylova M, Budinger E, Ohl FW, Stork O, Zenclussen AC, Karpova A, Schwegler H, Kreutz MR (2016) A Jacob/Nsmf Gene Knockout Results in Hippocampal Dysplasia and Impaired BDNF Signaling in Dendritogenesis. PLoS genetics 12:e1005907-e1005907. doi:10.1371/journal.pgen.1005907
39. Talantova M, Sanz-Blasco S, Zhang X, Xia P, Akhtar MW, Okamoto S, Dziewczapolski G, Nakamura T, Cao G, Pratt AE, Kang YJ, Tu S, Molokanova E, McKercher SR, Hires SA, Sason H, Stouffer DG, Buczynski MW, Solomon JP, Michael S, Powers ET, Kelly JW, Roberts A, Tong G, Fang-Newmeyer T, Parker J, Holland EA, Zhang D, Nakanishi N, Chen HS, Wolosker H, Wang Y, Parsons LH, Ambasudhan R, Masliah E, Heinemann SF, Pina-Crespo JC, Lipton SA (2013) Abeta induces astrocytic glutamate release, extrasynaptic NMDA receptor activation, and synaptic loss. Proc Natl Acad Sci U S A 110:E2518-2527. doi:10.1073/pnas.1306832110
40. Teich AF, Nicholls RE, Puzzo D, Fiorito J, Purgatorio R, Fa M, Arancio O (2015) Synaptic therapy in Alzheimer's disease: a CREB-centric approach. Neurotherapeutics 12:29-41. doi:10.1007/s13311-014-0327-5
41. Wang X, Blanchard J, Grundke-Iqbal I, Iqbal K (2015) Memantine Attenuates Alzheimer's Disease-Like Pathology and Cognitive Impairment. PLoS One 10:e0145441. doi:10.1371/journal.pone.0145441
42. Xia P, Chen HS, Zhang D, Lipton SA (2010) Memantine preferentially blocks extrasynaptic over synaptic NMDA receptor currents in hippocampal autapses. J Neurosci 30:11246-11250. doi:10.1523/jneurosci.2488-10.2010
43. Yiu AP, Rashid AJ, Josselyn SA (2011) Increasing CREB function in the CA1 region of dorsal hippocampus rescues the spatial memory deficits in a mouse model of

Alzheimer's disease. Neuropsychopharmacology 36:2169-2186. doi:10.1038/npp.2011.107

Figures

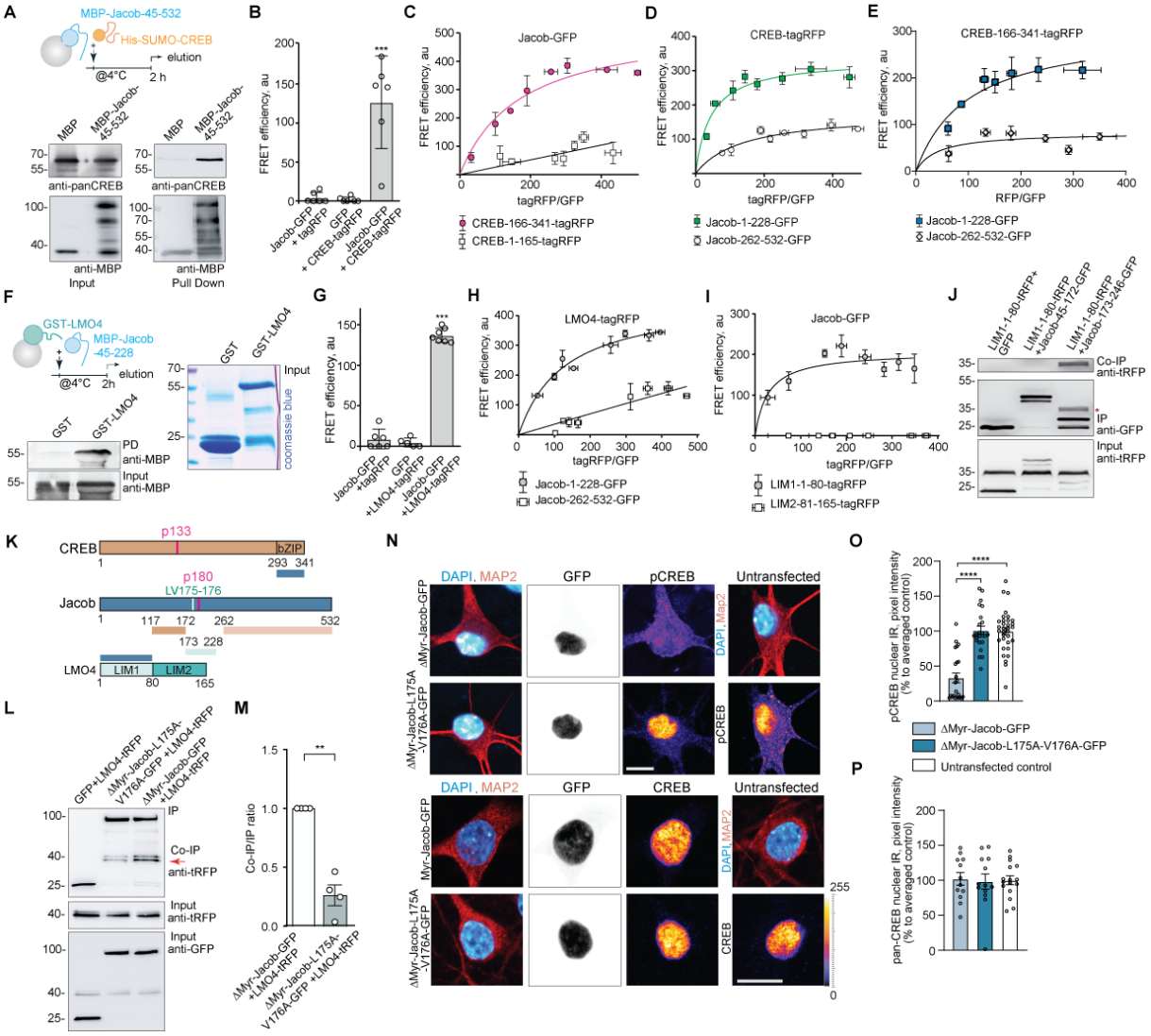

Fig. 1 Jacob directly associates with CREB and LMO4.

(A) Pull-down assay confirms a direct interaction of MBP-Jacob-45-532 and His-SUMO-CREB.
(B) FRET measurements show association between CREB-tagRFP and Jacob-GFP. Bar plot representing mean values of 5 independent experiments measured in triplicates ± SEM. ***p<0.001 by one-way ANOVA followed by Bonferroni's multiple comparisons test.
(C) The C-terminus but not the N-terminus of CREB closely associates with Jacob-GFP in FRET saturation experiments.
(D) FRET saturation experiments in cells expressing CREB-tagRFP and Jacob-1-228-GFP or Jacob-262-532-GFP revealed that both N- and C-termini of Jacob are in close proximity to CREB, however the Jacob-1-228-GFP association with CREB is significantly stronger.
(E) The C-terminus of CREB associates with both N- and C-termini of Jacob. However, association with Jacob-1-228-GFP is much stronger compared to its C-terminus (Jacob-262-532-GFP).
(B-E) FRET saturation experiments were performed in the HEK293T cell suspension. FRET efficiency is given in arbitrary units as a means of 5-6 independent experiments. Data are represented as mean ± SEM.

(F) The GST-LMO4 fusion protein but not control GST pulls down recombinant MBP-Jacob-45-228.
(G) FRET experiments in transfected HEK293T cells suspensions showing that Jacob-GFP interacts with LMO4-tagRFP. Bar plot representing mean values of 6 independent experiments measured in triplicates ± SEM. ***$p<0.001$ by one-way ANOVA followed by Bonferroni's multiple comparisons test.
(H, I) FRET saturation experiments indicating the association of Jacob-1-228-GFP with LIM-1-80-tagRFP. FRET efficiency is given in arbitrary units as a mean of 6 independent experiments. Data represented as mean ± SEM.
(J) Mapping for Jacob binding to the LIM1 domain of LMO4 reviled its association with 179-246 aa of Jacob, but not with Jacob-45-172-GFP (CREB-binding region).
(K) Scheme depicting domain organization and binding interfaces. Jacob binds to the bZIP domain of CREB (blue box). The orange box indicates a stronger interaction of the Jacob N-terminus, the shaded orange box indicates a weaker association of the C-terminus. The LIM1 domain of LMO4 (dark blue box) binds to 173-228 aa of Jacob (light blue box).
(L, M) Leucine at position 175 is crucial for the association of Jacob with LMO4. Heterologous co-immunoprecipitation experiments between LMO4-tagRFP and nuclear ΔMyr-Jacob-GFP, ΔMyr-Jacob-L175A-V176A-GFP or GFP overexpressed in HEK293T cells revealed decreased association of ΔMyr-Jacob-L175A-V176A-GFP with LMO4 compare to ΔMyr-Jacob-GFP. **$p<0.01$ by one-sample t-test from 4 independent experiments.
(N-P) A Jacob-LMO4-binding mutant expressed in the nucleus does not induce CREB shut-off. **(N, O)** Representative confocal images of hippocampal neurons transfected with ΔMyr-Jacob-GFP or ΔMyr-Jacob-L175A-V176A-GFP. Scale bar: 10 µm. **(P)** Dot plots representing mean of nuclear pCREB immunoreactivity in Jacob-expressing neurons normalized to untransfected control. "N" - the number of neuronal nuclei analyzed from two independent cell cultures. Data are represented as mean ± SEM. ****$p<0.0001$ by one-way ANOVA followed by Tukey's multiple comparisons test.

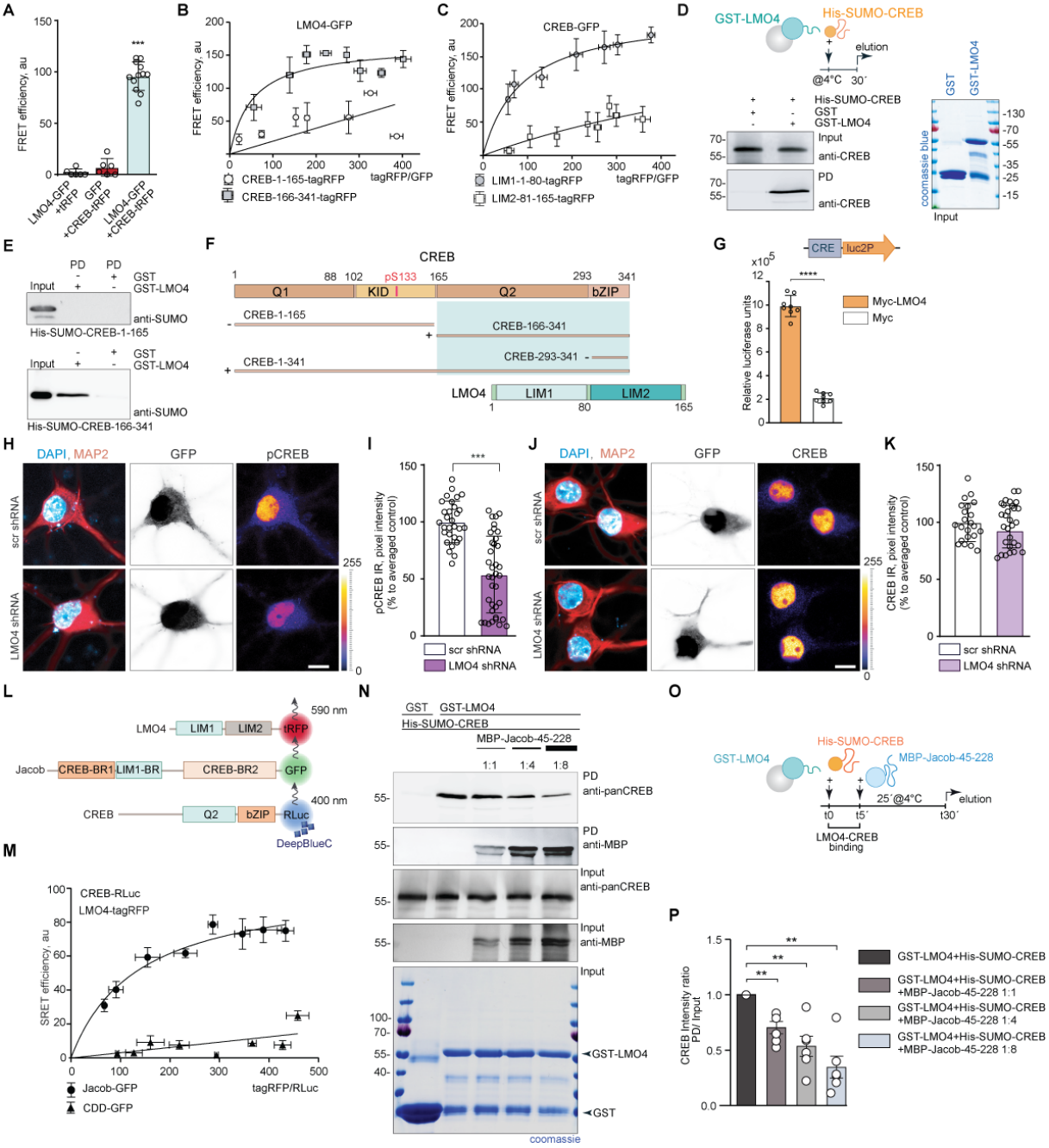

Fig. 2 Jacob displaces LMO4 from CREB.

(A) FRET measurements indicate a tight association between LMO4-GFP and CREB-tagRFP expressed in HEK293T cells. Bar plot representing mean values of 6 independent experiments measured in triplicates ± SEM, ***p<0.001 by one-way ANOVA followed by Bonferroni's multiple comparisons test.

(B, C) FRET saturation experiments with **(B)** LMO4-GFP and CREB-1-165-tagRFP or **(C)** CREB-166-341-tagRFP and CREB-GFP and LIM1-1-80-tagRFP or LIM2-81-165-tagRFP revealed the association between LIM1 domain of LMO4 and C-terminus of CREB. Box plots of FRET arbitrary units from 8 independent experiments. Data represented as mean ± SEM.
(D) Bacterially produced recombinant His-SUMO-CREB directly binds to GST-LMO4 in pull-down experiments. Cartoon represents the scheme of the experiment.

(E) The interaction between CREB with LMO4 is mediated by the C-terminus of CREB (166-341 aa), but not by its N-terminus (1-165 aa). Pull-down experiments between recombinant His-SUMO-1-165-CREB, His-SUMO-166-341-CREB and GST-LMO4.
(F) Schematic representation of CREB and LMO4 domain structure and fusion constructs used for the experiments. Light green boxes represent the interaction interface.
(G) Myc-LMO4 overexpression increases CREB dependent luciferase expression in HEK293T cells stably transfected with pGL4.29 [luc2P/CRE/Hygro] vector expressing luciferase under the CRE promoter. Depicted are the relative luciferase units in cells overexpressing Myc-LMO4 as compared to Myc-transfected controls. N=8, from two independent experiments. Data are represented as mean ± SEM. ****$p<0.0001$ by two-tailed Student t-test.
(H-K) Knockdown of LMO4 reduces nuclear pCREB immunoreactivity. **(H, J)** Representative confocal images of hippocampal neurons transfected with LMO4 shRNA construct or scrambled control (both expressing GFP under CMV promoter as a transfection control). Scale bar: 10µm. Dot plots representing the mean of nuclear **(I)** pCREB or **(K)** CREB staining intensity normalized to scrambled control. "N"- the number of nuclei analyzed from at least 3 independent cell cultures. Data are represented as mean ± SEM. ***$p<0.001$ by two-tailed Student's t-test.
(L, M) SRET saturation experiments reveal that Jacob-GFP can form a triple complex with CREB-RLuc and LMO4-tagRFP. HEK293T cells were transfected with CREB-RLuc and LMO4-tagRFP and **(L)** Jacob-GFP or CDD-GFP (negative control). Data represented as mean ± SEM of 8 independent experiments. SRET saturation curve indicates binding between respective proteins while straight line represents no interaction. **(M)** Schematic representation of constructs used in SRET experiments. "BR" stands for binding region.
(N-P) The N-terminus of Jacob displaces LMO4 from CREB. Schematic depicts the timeline of the competition pull-down experiment where GST-LMO4 coupled to beads was preincubated with His-SUMO-CREB and subsequently incubated with an enhanced amount of MBP-Jacob-45-228. **(N)** Immunoblot developed with anti-CREB and anti-MBP antibodies showing decreased intensity for the CREB band upon increasing concentration of MBP-Jacob-45-228. **(O)** The image of a coomassie blue stained gel represents GST-LMO4 and GST control coupled to beads. **(P)** Quantification of CREB band intensity normalized to the input (n=6). Data represented as mean ± SEM. **$p<0.01$ by one-sample t-test.

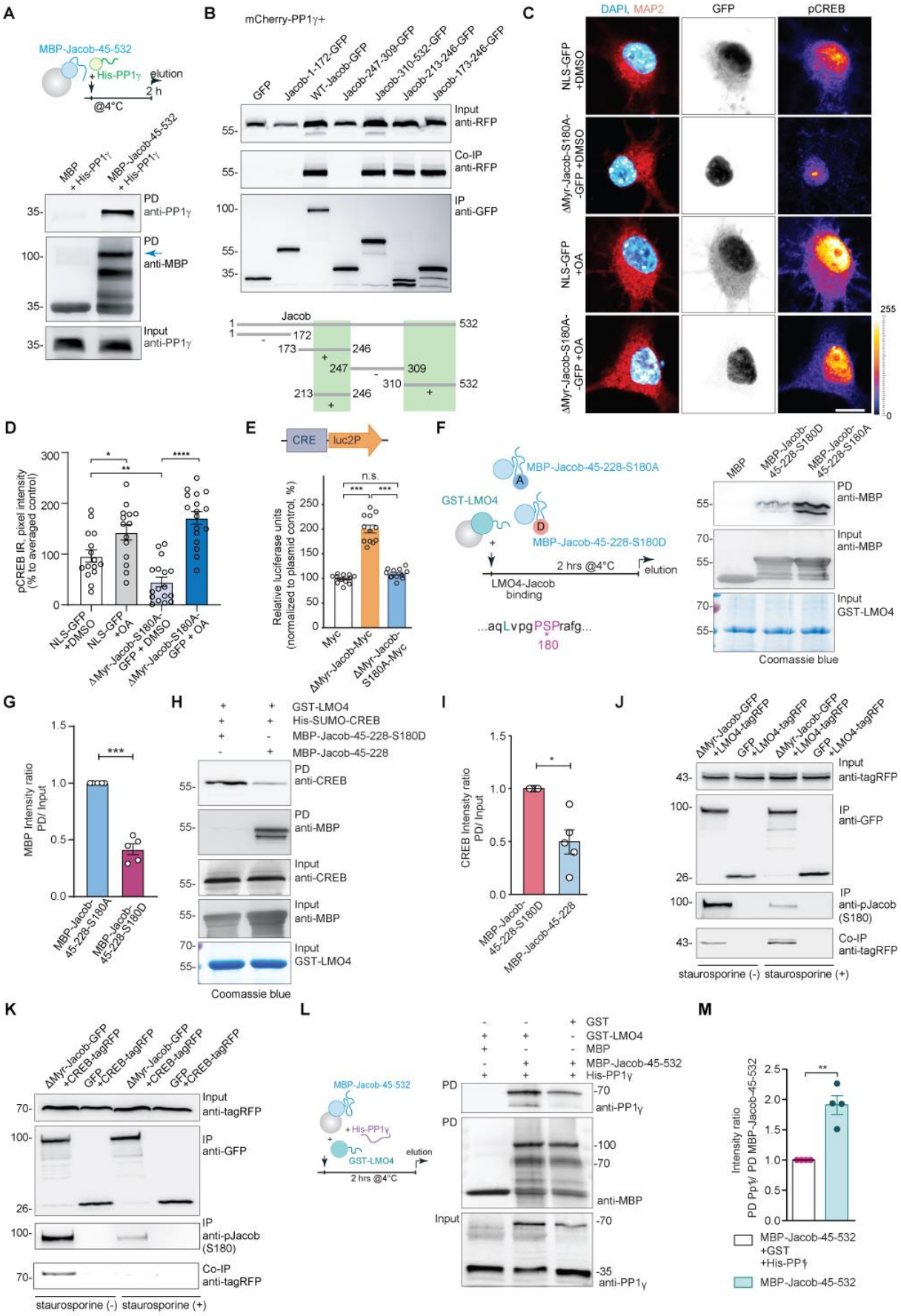
A
MBP-Jacob-45-532
+His-PP1γ
elution
2 h
@4°C
MBP + His-PP1γ
MBP-Jacob-45-532 + His-PP1γ
PD anti-PP1γ
PD anti-MBP
Input anti-PP1γ
B
mCherry-PP1γ+
GFP
Jacob-1-172-GFP
WT-Jacob-GFP
Jacob-247-309-GFP
Jacob-310-532-GFP
Jacob-213-246-GFP
Jacob-173-246-GFP
Input anti-RFP
Co-IP anti-RFP
IP anti-GFP
Jacob
C
DAPI, MAP2
GFP
pCREB
NLS-GFP +DMSO
ΔMyr-Jacob-S180A--GFP +DMSO
NLS-GFP +OA
ΔMyr-Jacob-S180A--GFP +OA
D
pCREB IR, pixel intensity (% to averaged control)
NLS-GFP +DMSO
NLS-GFP +OA
ΔMyr-Jacob-S180A-GFP + DMSO
ΔMyr-Jacob-S180A-GFP + OA
E
CRE
luc2P
Relative luciferase units (normalized to plasmid control, %)
n.s.
Myc
ΔMyr-Jacob-Myc
ΔMyr-Jacob-S180A-Myc
F
MBP-Jacob-45-228-S180A
GST-LMO4
MBP-Jacob-45-228-S180D
2 hrs @4°C
elution
LMO4-Jacob binding
...aqLvpgPSPrafg...
180
MBP
MBP-Jacob-45-228-S180D
MBP-Jacob-45-228-S180A
PD anti-MBP
Input anti-MBP
Input GST-LMO4
Coomassie blue
G
MBP Intensity ratio PD/ Input
MBP-Jacob-45-228-S180A
MBP-Jacob-45-228-S180D
H
GST-LMO4
His-SUMO-CREB
MBP-Jacob-45-228-S180D
MBP-Jacob-45-228
PD anti-CREB
PD anti-MBP
Input anti-CREB
Input anti-MBP
Input GST-LMO4
Coomassie blue
I
CREB Intensity ratio PD/ Input
MBP-Jacob-45-228-S180D
MBP-Jacob-45-228
J
ΔMyr-Jacob-GFP +LMO4-tagRFP
GFP +LMO4-tagRFP
Input anti-tagRFP
IP anti-GFP
IP anti-pJacob (S180)
Co-IP anti-tagRFP
staurosporine (-)
staurosporine (+)
K
ΔMyr-Jacob-GFP +CREB-tagRFP
GFP +CREB-tagRFP
Input anti-tagRFP
IP anti-GFP
IP anti-pJacob (S180)
Co-IP anti-tagRFP
staurosporine (-)
staurosporine (+)
L
MBP-Jacob-45-532
+His-PP1γ
GST-LMO4
elution
2 hrs @4°C
GST
GST-LMO4
MBP
MBP-Jacob-45-532
His-PP1γ
PD
anti-PP1γ
anti-MBP
Input
anti-PP1γ
M
Intensity ratio PD Pp1γ/ PD MBP-Jacob-45-532
MBP-Jacob-45-532 +GST +His-PP1γ
MBP-Jacob-45-532

Fig. 3 CREB shut-off essentially requires Jacob binding to PP1.

(A) Pull-down experiments confirmed a direct interaction between bacterially produced recombinant MBP-Jacob-45-532 and His-PP1γ.
(B) Mapping of the PP1γ interaction region within the Jacob sequence revealed binding of a C-terminal fragment (Jacob-310-250-GFP) as well as the N-terminal part (Jacob-173-246-GFP) where the region between 213-246 aa is sufficient for immunoprecipitation. Immunoblot represents heterologous Co-IP from HEK293T cells transfected with mCherry-PP1γ and different fragments of Jacob fused with GFP or GFP alone. The scheme represents the different Jacob fragments used for CoIP. Green boxes indicate interaction regions.
(C, D) Treatment of hippocampal primary neurons expressing phosphodeficient mutant Jacob in the nucleus with okadaic acid rescues Jacob-induced CREB shut-off. Confocal images of pCREB immunostaining in DIV15 neurons overexpressing ΔMyr-Jacob-S180A-GFP with and without OA treatment. Scale bar: 20 μm. "N"- the number of nuclei analyzed from 2 independent cell cultures. Data represented as mean ± SEM. ****$p<0.0001$ vs. non-transfected control by repeated measures two-way ANOVA followed by two-tailed Student's t-test.
(E) Overexpression of ΔMyr-Jacob-Myc but not the phospho-deficient mutant (ΔMyr-Jacob-S180A-Myc) positively regulates CREB dependent expression of luciferase measured as luciferase activity in a stably transfected HEK293T cell line (pGL4.29[luc2P/CRE/Hygro] Vector). Data are represented as mean ± SEM from 3 independent experiments. ***$p<0.001$ by one-way ANOVA followed by Bonferroni's multiple comparisons test.
(F, G) Phosphodeficient N-terminus of Jacob (MBP-Jacob-45-228-180A) interacts with LMO4 stronger than its phosphomimetic form (MBP-Jacob-45-228-180D). The scheme depicts the experimental outline, where bacterially expressed GST-LMO4 immobilized on beads was incubated with either MBP-Jacob-45-228-180A or MBP-Jacob-45-228-180D. **(G)** Bar graph represents quantification of MBP immunoreactivity normalized to input. N=5, ***$p<0.001$ by one-sample t-test.
(H, I) Phosphomimetic Jacob mutant (MBP-45-228-180D) is unable to displace LMO4 from CREB. Recombinant GST-LMO4 was coupled to beads, preincubated with His-SUMO-CREB and subsequently incubated in 1:8 ratio with MBP-Jacob-45-228 or MBP-45-228-180D. Immunoblot developed with anti-CREB antibody. The image of coomassie blue stained gel represents the GST-LMO4 input. **(I)** Quantification of the CREB band intensity normalized to the input. N=5. Data represented as mean ± SEM. *$p<0.05$ by one-sample t-test.
(J) Treatment with staurosporine decreases Jacob phosphorylation level (S180), but increases its association with LMO4-tagRFP. Immunoblot of HEK293T cells extracts transfected with LMO4-tagRFP and ΔMyr-Jacob-GFP or GFP alone.
(K) Treatment with staurosporine decreases the association of Jacob with CREB. Immunoblot of HEK293T cells extract transfected with CREB-tagRFP and ΔMyr-Jacob-GFP or GFP as a control.
(L, M) The association of Jacob with LMO4 enhances its interaction with PP1γ in pull-down assays. **(L)** PP1γ interacts with Jacob as a dimer (70 kDa) that forms during purification. **(M)** Bar graph represents quantification of PP1γ immunoreactivity normalized to MBP-Jacob. N=4, **$p<0.01$ by one-sample t-test.

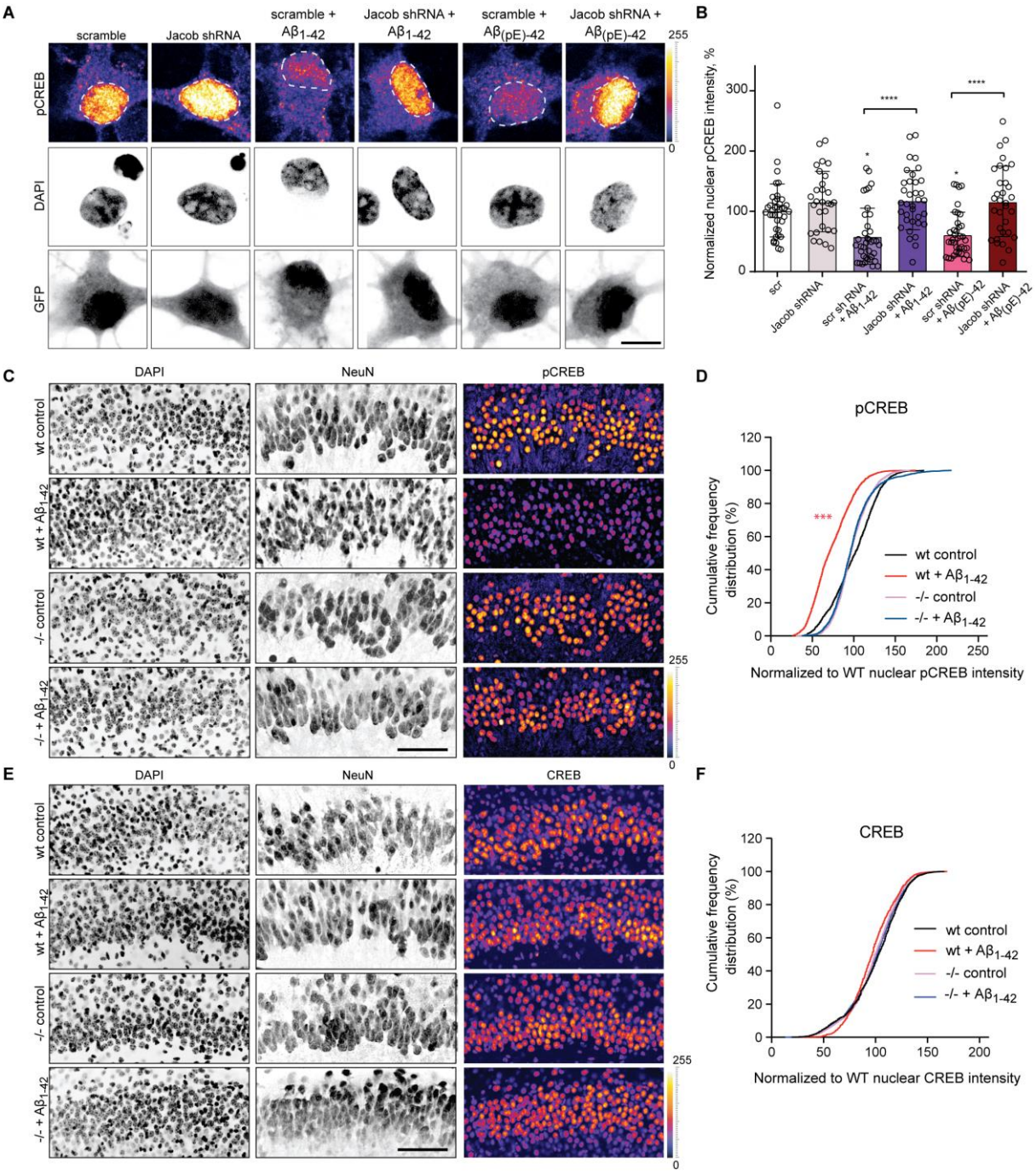

Fig. 4 Jacob mediates Aβ-induced CREB shut-off.

(A, B) Jacob shRNA knockdown prevents Aβ-induced CREB shut-off. Representative confocal images of hippocampal neurons transfected with Jacob-shRNA construct or scrambled (scr) shRNA control (both expressing GFP) and treated with oligomeric preparations of $A\beta_{1-42}$ or $A\beta_{3(pE)-42}$. **(B)** Contrary to the scr shRNA, neurons transfected with Jacob knockdown construct did not display reduction of pCREB staining intensity after treatment with $A\beta_{1-42}$ or $A\beta_{3(pE)-42}$. Bar plot of mean nuclear pCREB intensity normalized to scramble untreated control. Scale bar: 10 µm. N=29-39 nuclei from 2 independent experiments. ****$p<0.0001$ by 2way ANOVA followed by Sidak's multiple comparisons test, *$p<0.05$ by two-way ANOVA followed by Tukey's multiple comparisons test. Data are represented as mean ± SEM.

(C-F) Acute (1h) Aβ_{1-42} treatment does not induce CREB shut-off in organotypic hippocampal slices from Jacob knock-out mice. Representative confocal images of slices immunolabeled against pCREB **(C)** or panCREB **(E)**, co-labeled with anti-NeuN antibody and co-stained with DAPI. Cumulative frequency distribution of pCREB **(D)** and panCREB **(F)** nuclear staining intensity. **(D)** N=2320-3669 nuclei from 16-22 slices. **(F)** N=1177-2079 nuclei from 11-14 slices. ***p<0.001 by two-way ANOVA followed by Tukey's multiple comparisons test. Lookup tables **(A,C,E)** indicate the pixel intensities from 0 to 255.

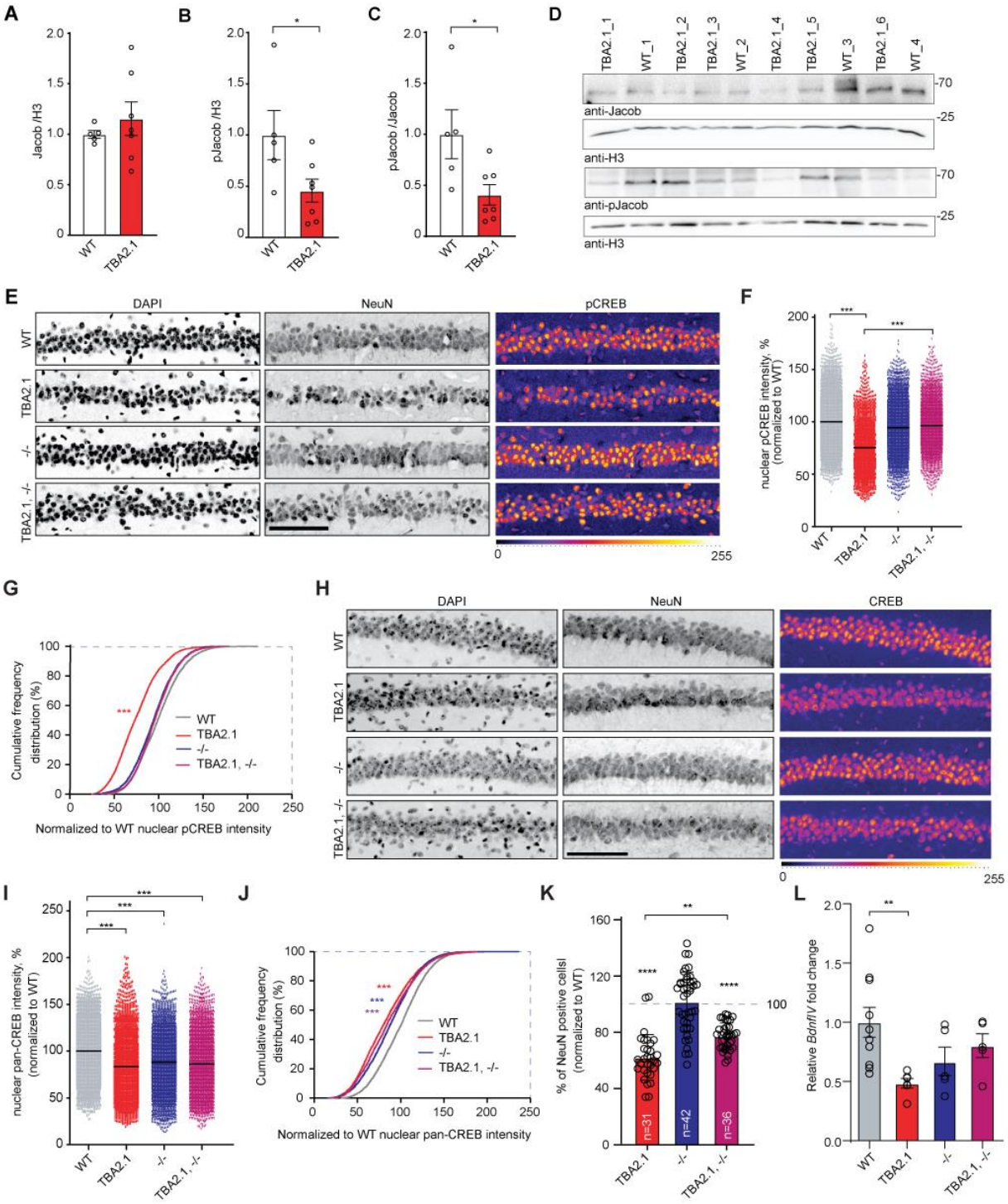

Fig. 5 Jacob regulates CREB function and neuronal loss in an animal model of Alzheimer's disease.

(A-C) pJacob level and pJacob/panJacob ratio are decreased in TBA2.1 mouse line compared to WT animals. **(A)** Quantification of Jacob level, **(B)** pJacob level and **(C)** pJacob/Jacob ratio normalized to Histone3 (H3). N=5-7 hippocampal, protein extracts. *p<0.05 by two-tailed Student t-test. Data are represented as mean ± SEM.
(D) Representative images of immunoblots probed with antibodies against pJacob (S180), panJacob and Histone3.
(E) Representative confocal images of distal CA1 cryosections from 12 weeks old mice stained for NeuN, DAPI and pCREB. Scale bar: 100 µm.
(F, G) The quantification of pCREB intensity in NeuN-positive cells revealed a statistically significant decrease in pCREB immunoreactivity in TBA2.1 but not in double transgenic animals (TBA2.1, -/-). Data are represented as **(F)** dot plot and **(G)** cumulative frequency distribution. N=655-1232 nuclei from 7-9 animals. ***p<0.001 by two-way ANOVA followed by Bonferroni's multiple comparisons test. Data are represented as mean ± SEM.
(H) Confocal images were averaged from two sections of the nuclear layer of distal CA1 stained for NeuN, DAPI and CREB. Scale bar: 100 µm.
(I, J) The quantification of CREB intensity in NeuN positive cells revealed a statistically significant decrease in CREB immunoreactivity in Jacob/*Nsmf* knock-out (-/-) and TBA2.1 Jacob/*Nsmf* knock-out (TBA2.1, -/-) mice. Data are represented as **(I)** dot plot and **(J)** cumulative frequency distribution of CREB nuclear staining intensity. N=1668-3073 nuclei from 7-9 animals **(J)**. ***p<0.001 by two-way ANOVA followed by Bonferroni's multiple comparisons test.
(K) Both TBA2.1 and TBA2.1 Jacob/*Nsmf* knock-out animals (TBA2.1, -/-) display neuronal loss in CA1 region of hippocampus. Bar plot representing the number of NeuN positive cells normalized to WT group. The TBA2.1 Jacob/*Nsmf* knock-out (TBA2.1, -/-) mice display significantly lower degree of neuronal loss compared to TBA2.1 mice. N=31-42 CA1 images analyzed from 9-11 animals per genotype. ****p<0.0001, **p<0.01 by two-way ANOVA followed by Bonferroni's multiple comparisons test. Data are represented as mean ± SEM. Lookup tables indicate the pixel intensities from 0 to 255 **(E, H)**.
(L) Jacob knock-out rescues decrease in the *BdnfIV* gene transcription. Bar plot of mean *BdnfIV* transcript levels in hippocampal homogenates normalized to β-actin as a reference gene. N=5-10 hippocampi. **p<0.01 by two-way ANOVA followed by Bonferroni's multiple comparisons test. Data are represented as mean ± SEM.

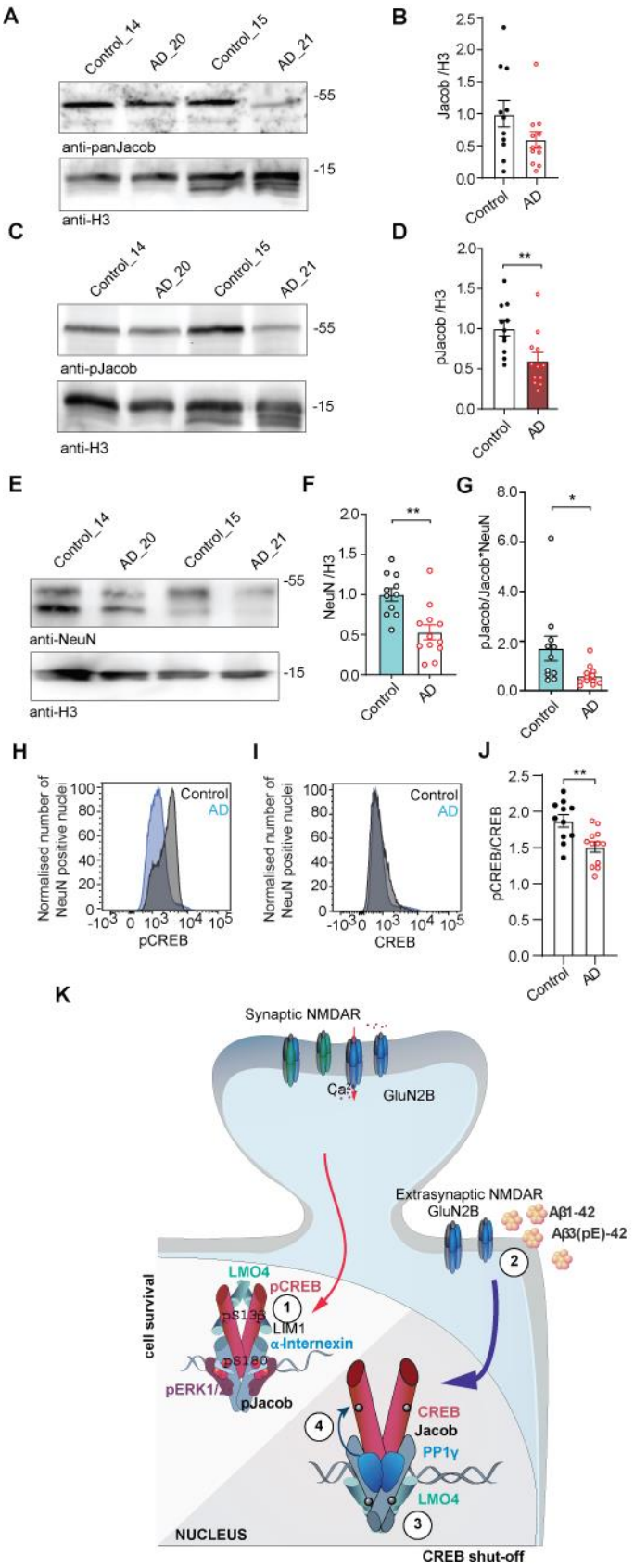

Fig. 6 pJacob is decreased in Alzheimer's disease patients which correlates with decreased nuclear pCREB.

(A, B) Total Jacob protein levels are not significantly reduced in brain samples from Alzheimer's disease patients as compared to the control group.

(C, D) pJacob, **(E, F)** NeuN, as well as **(G)** pJacob/panJacob ratio by NeuN is decreased in brain samples from AD patients as compared to the control group. **(A, C, E)** Representative images of the immunoblot probed with antibodies against pJacob, pan-Jacob, NeuN and re-probed with Histone3 (H3). The protein quantification was normalized to H3. **(B, D, F, G)** Bar plots representing the quantification of WB immunodensity for particular proteins normalized to H3 and control patients. N=11-12 protein extracts from different subjects. *$p<0.05$, **$p<0.01$ by two-tailed Student t-test. Data are represented as mean ± SEM.
(H-J) FACS measurements revealed significantly decreased pCREB, but not CREB, immunoreactivity of neuronal nuclei in AD patients as compared to the control group. **(H, I)** Frequency distribution plot of neuronal nuclei immunoreactivity of **(H)** pCREB and **(I)** CREB. **(J)** Bar plot representing quantification of pCREB/CREB ratio in neuronal nuclei. N=11-12 protein extracts from different subjects. **$p<0.01$ by two-tailed Student t-test.
(K) Jacob docks a signalosome to CREB that encodes the synaptic (1) or extrasynaptic (2) origin of the NMDAR signal. Following synaptic NMDAR activity Jacob docks the MAP-kinase ERK to CREB which results in sustained CREB activation (1). In case of disease-related stimulation of extrasynaptic NMDAR with amyloid-β dephosphorylated Jacob associates with the CREB adaptor protein LMO4 and replaces it from the CREB complex (3). In parallel, the association with LMO4 enhances binding of Jacob to PP1γ and this complex induces long-lasting dephosphorylation and transcriptional inactivation of CREB in the context of early synaptic dysfunction and cell loss in Alzheimer's disease (4).

Supplementary Materials

Supplementary methods

Virus production and NMDA-induced CREB shut-off

The lentivirus was produced in the HEK293T cell line (Lenti-X 293T, Clontech). Cells were transfected with FUGW-based transfer shRNA, psPAX2 packaging, and pVSVG pseudotyping vectors using calcium phosphate method with a molar ratio of FUGW: psPAX2: pVSVG: 2:1:1. After 12-16h of transfection, cells were cultured in low serum DMEM (Gibco) supplemented with 4% FBS (Gibco). The virus was harvested from the culture media after 48h by ultracentrifugation at a speed of 20000rpm for 2h at 4°C. The virus pellet was resuspended in 100µl of Neurobasal media by shaking at 300rpm for 55min. Resuspended virus was collected and spun again at 14000rpm for 5min. The supernatant was aliquoted and stored at -80°C.

For NMDA-induced CREB shut-off experiments previously described protocol was used [34]. Briefly, DIV7 cultures were infected with lentivirus carrying Jacob knockdown or scrambled construct for 12 h. At DIV16, cells were silenced overnight with 1 µM tetrodotoxin (TTX, Carl Roth) and on the following day after TTX washout cultures were treated with 100µM Forskolin (Biorbyt), 10µM Nifedipine (calcium channel blocker, Santa Cruz), and 40µM CNQX (Tocris). After 30 min, 100µM of NMDA (Sigma-Aldrich) was added directly into the culture media for 2, 5, 10, and 15min. 2xSDS sample buffer with protease and phosphatase inhibitor was directly added to the wells to stop the NMDA mediated CREB shut-off and lyse the cells. Samples were subjected for the WB analysis.

For multielectrode array experiments the semliki forest virus was prepared as described previously [21].

Cell death experiments on the OHSC

Before cell death experiments, the viability of slices was assessed by adding 2µM propidium iodide (PI) for several h directly into the culture medium.

For oxygen-glucose deprivation (OGD)-induced cell death experiment membranes with OHSC were transferred to 1ml OGD medium (Ringer solution with 10mM mannitol or 10 mM glucose as a control) with 3µM PI. Next, cultures were exposed to 10 min of 95% N_2/5% CO_2 gas flow in a hypoxic chamber (Billupsand Rothenberg) and kept in the reduced O_2 conditions for 30min at 35ºC. Afterwards, the membranes were moved back to their previous medium containing 3µM PI and imaged at the indicated time points.

For NMDA-induced cell death experiment OHSC were transferred to the medium containing 50µM NMDA (Sigma-Aldrich) and 3µM PI. Afterwards, membranes were moved back to their previous medium containing 3µM PI and imaged at the time points indicated in figure legend. To prove that the observed cell death is NMDAR-dependent, slices were pre-incubated with 10µM MK-801 (Sigma-Aldrich) for 1h and during the NMDA exposure. To assess the cell death the images of red PI fluorescence and bright field images were acquired with a Zeiss Axioskop 2 with the 4x objective using Nikon NIS software. The CA1, C3, and DG regions of interest (ROIs) were defined based on the bright-field image. Mean pixel intensity was measured in grey-scale images, and individually baseline-corrected for time point 0 (directly after the experiment). The analysis was done by an experimenter blind to genotype and treatment group. For representative images, PI images of different time points were aligned using the Fiji plugin linear stack alignment with SIFT and default settings in the rigid mode. Represented images are contrast-enhanced (equally for all groups). PI/ImageJ uptake was imaged at the time points indicated in the figure legend.

Characterization of anti-panJacob and pJacob(S180) antibodies for the detection of human protein

For initial characterization of anti-panJacob and pJacob(S180) antibodies for the detection of human protein HEK293T cells were transfected with the plasmid expressing hJacob-SPOT. Overexpressed protein was immunoprecipitated from the cell lysate using tag specific nano-trap (SPOT-Trap-MA, Chromotek) and analysed by WB.

Cell based co-recruitment assay

HEK293T cells were transfected with respective constructs (Table S2). On the following day cells were fixed with 4% PFA, permeabilized with 0,1% TX-100 in 1xPBS for 10min, stained with DAPI and mounted. Z-stack with 300nm step size was taken with 512x512 pixels format using a Leica TCS SP8-STED system. Maximal intensity images from three optical sections were generated for representative images.

Stimulated emission depletion (STED) microscopy

STED images were obtained using a Leica TCS SP8 STED 3X equipped with pulsed White Light Laser (WLL) and diode 405nm laser for excitation and pulsed depletion laser 775 nm and Leica HC ApoCS2 100x/1.40 oil objective. MAP2 and DAPI were acquired in confocal mode. The pixel size for all images was 20-23 nm (XY-plane). The Z-step was 150nm. STED

and confocal images were deconvolved using Deconvolution wizard (Huygens Professional, SVI), with optimized iteration method. Intensity profiles were created in Fiji/ImageJ.

Multielectrode array (MEA)

Dissociated hippocampal neurons were plated on Poly-D-lysine coated microelectrode arrays (MEA60 200Pt GND, Ayanda Biosystems SA, Switzerland) with a plating density of 500 000 cells per array and cultured in NB medium at 37°C for at least 19 days. 12h prior to baseline recording HEPES buffer was added at a final concentration of 10 µM. For extracellular recording of spontaneous network activity, MEAs were connected to an amplifier (MEA1060-INV-BC, MultiChannel Systems, Germany), which was placed in a non-humidified incubation chamber (Solent scientific, Germany) mounted on an Olympus IX81 inverted microscope and maintained at 37°C. Subsequently, after recording the baseline network activity cultures were infected with semliki forest virus bearing nuclear phosphomimetic or nuclear phosphodeficient Jacob as well as GFP for control and placed back to the humidified incubator. Eight to nine hours after infection, network activity recording was repeated. Derived neuronal activity was digitized at 10 kHz using MC_Rack software (MutiChannel Systems, Germany). Acquired raw records were high-pass filtered (gain 300 Hz) and used for threshold-based spike detection (±5 standard deviations computed for ~1 s long spike-free period separately for each individual channel) and burst identification (minimum 5 spikes per burst with maximal interval between spikes of 100 ms). The data for each culture were normalized to respective baseline. Treatment and analysis of multi-channel records of neuronal activity was carried out using Spike2 software (Cambridge Electronic Design Ltd, UK).

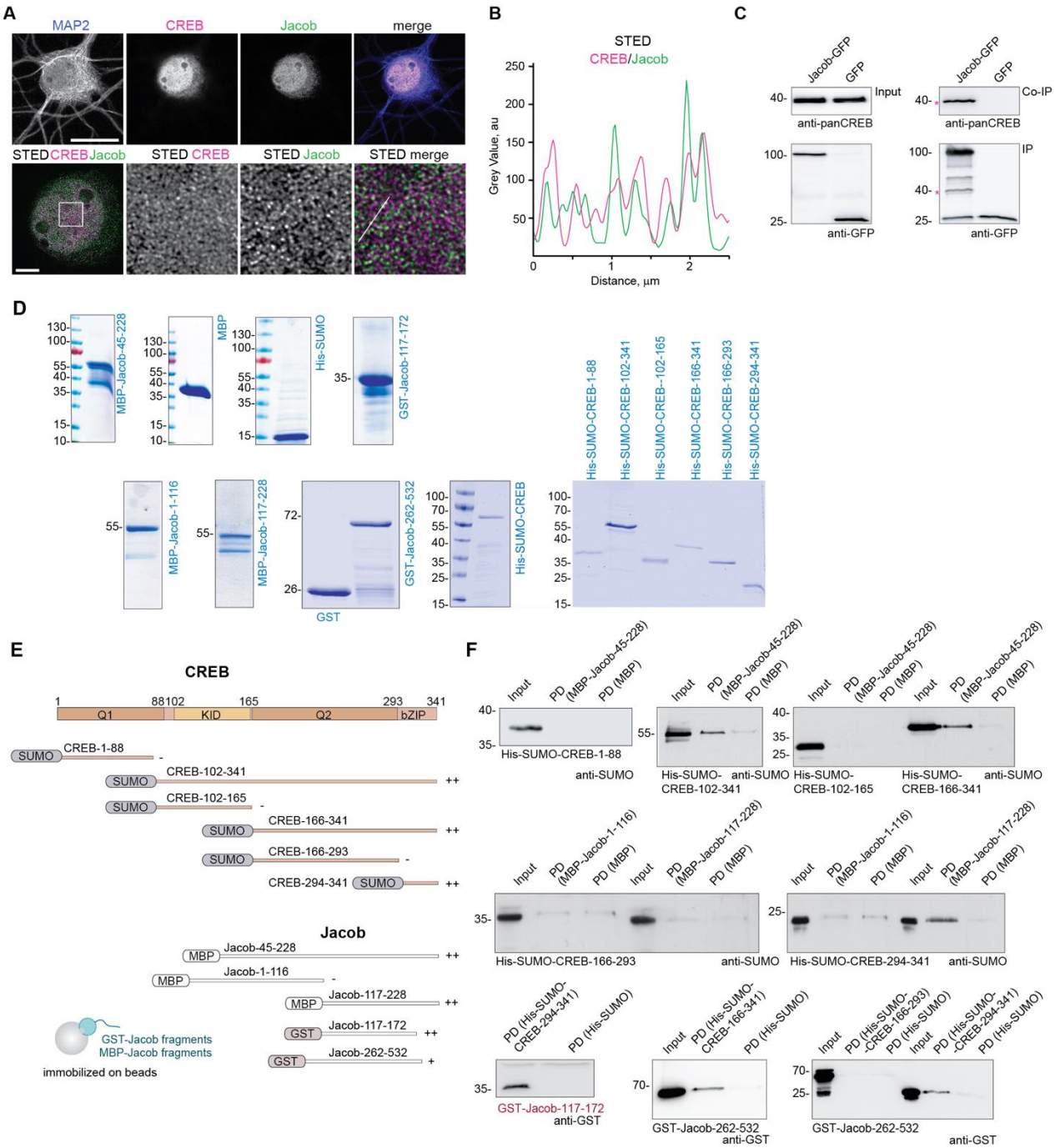

Fig. S1 (refers to Fig. 1) Confirmation of Jacob-CREB interaction, mapping of the binding interfaces between Jacob and CREB.

(A, B) Confocal and STED images show an association of CREB with Jacob in the nucleus of DIV16 hippocampal primary neurons. **(A)** The upper panel represents deconvolved confocal images. Lower panels depict deconvolved STED images. Scale bars: 20 µm and 5 µm respectively. Inserts are denoted by a white square. **(B)** Line profiles indicate the overlap of relative intensities for CREB and Jacob along a 2,5 µm line.

(C) Endogenous CREB co-immunoprecipitates with overexpressed Jacob-GFP, but not GFP from HEK293T cell extracts. The asterisk denotes the CREB band from a membrane subsequently re-probed with an anti-GFP antibody.

(D) Coomassie blue staining depicting the purity of bacterially produced proteins used for pull-down assays between CREB and Jacob.

(E) Scheme representing the constructs used for mapping of the interaction sites in Fig. 1D and S1B.
(F) The N-terminus of Jacob (117-172 aa in red) interacts with the bZIP domain of CREB, but not with the Q1 (1-88 aa), KID (102-165 aa), or Q2 (166-293 aa) domains. The C-terminus of Jacob (262-532 aa) shows weaker binding to the bZIP domain of CREB. Images of immunoblots representing pull-down assays performed with Jacob and CREB protein fragments depicted in the panel B.

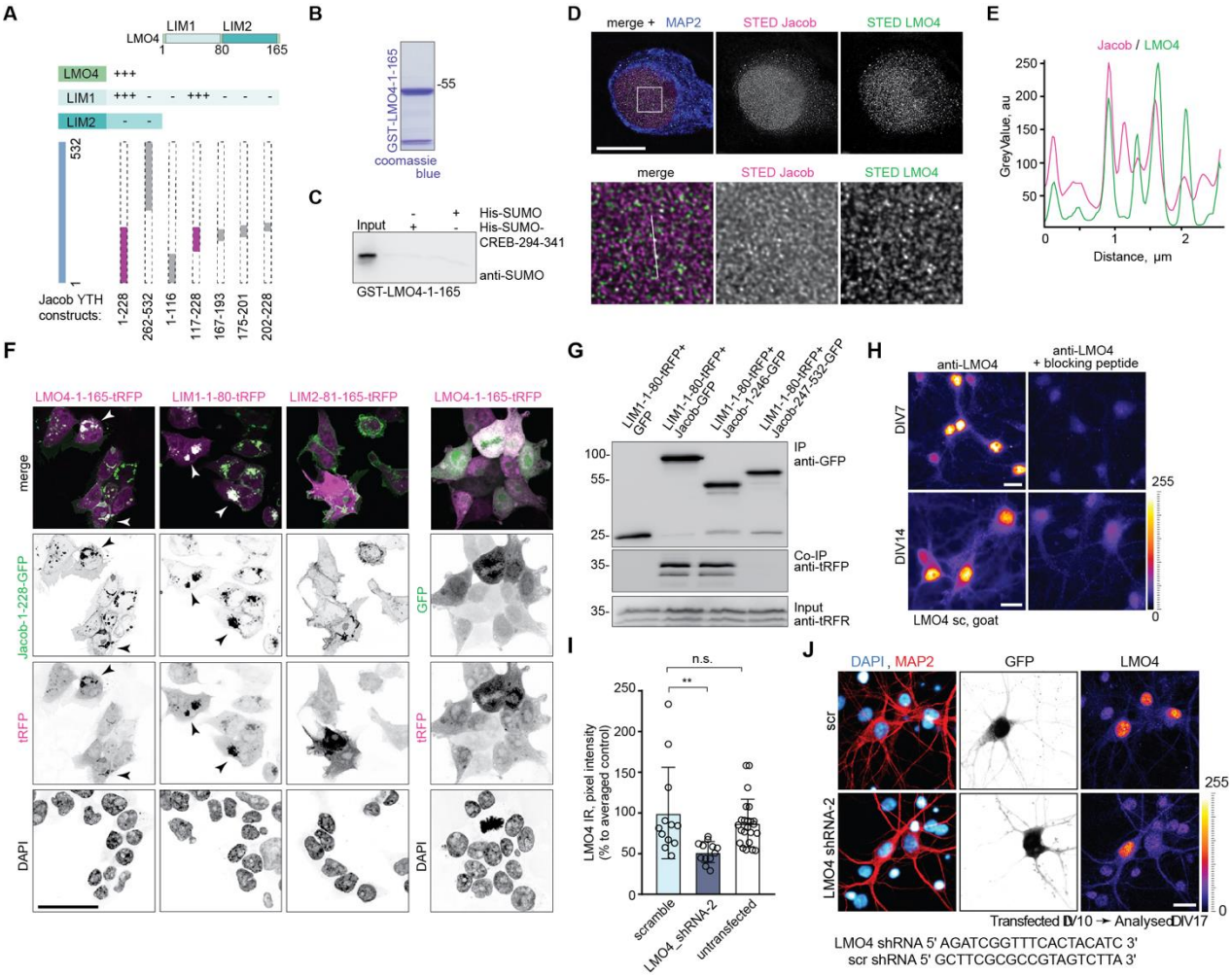

Fig. S2 (refers to Fig. 1 and 2) Confirmation of LMO4-Jacob interaction, LMO4 antibody specificity and quantification of LMO4 knockdown efficiency.

(A) Jacob-117-228 interacts with the LIM1 domain of LMO4 in Y2H. (+++) indicates a strong interaction while (–) indicates no interaction. Evaluation was based on the number of colonies growing in triple drop-out media.
(B) Coomassie blue stained gel showing purity of GST-LMO4 used in the pull-down experiments.
(C) Pull-down experiments revealed no interaction between His-SUMO-CREB-294-341 with GST-LMO4.
(D, E) Super-resolution STED imaging revealed association of Jacob with LMO4 in the nucleus **(D)**. DIV16 primary hippocampal neurons stained with antibodies against MAP2, LMO4, pan-Jacob. Upper panel - scale bar:10 µm, lower panel (inserts 5 µm x5 µm – denoted by the white square). **(E)** Line profiles indicate relative intensities for deconvolved STED channels along a 2.5 µm line.

(F) Jacob-1-228-GFP co-recruits the LIM1 (1-80), but not LIM2 (81-165) domain of LMO4. Confocal images of HEK293T cells co-transfected either with Jacob-1-228-GFP or GFP together with LMO4 constructs. Arrows indicate co-recruitment. Scale bar: 40 µm.
(G) LIM1-1-80-tRFP co-immunoprecipitates with Jacob-1-246-GFP, but not Jacob-247-532-GFP from HEK293T cell extracts.
(H) A goat C-15 LMO4 antibody (Santa Cruz) was used to stain LMO4 in hippocampal neurons (DIV 7 and DIV 14) in the presence or absence of the blocking peptide. Scale bars: 15 µm.
(I) Representative, confocal images of hippocampal neurons transfected with shRNA targeting LMO4 or scrambled control. Reduction of nuclear LMO4 level was confirmed in immunocytochemistry with the goat anti-LMO4 (sc C-15). Scale bar:10 µm.
(J) Nuclear LMO4 staining intensity was downregulated in neurons expressing shRNA targeting LMO4 mRNA compared to scrambled-transfected (scr shRNA) or non-transfected cells. Data represented as mean ± SEM. n=12-23 nuclei. **p<0,021 by Kruskal-Wallis test followed by Dunn's multiple comparison test.

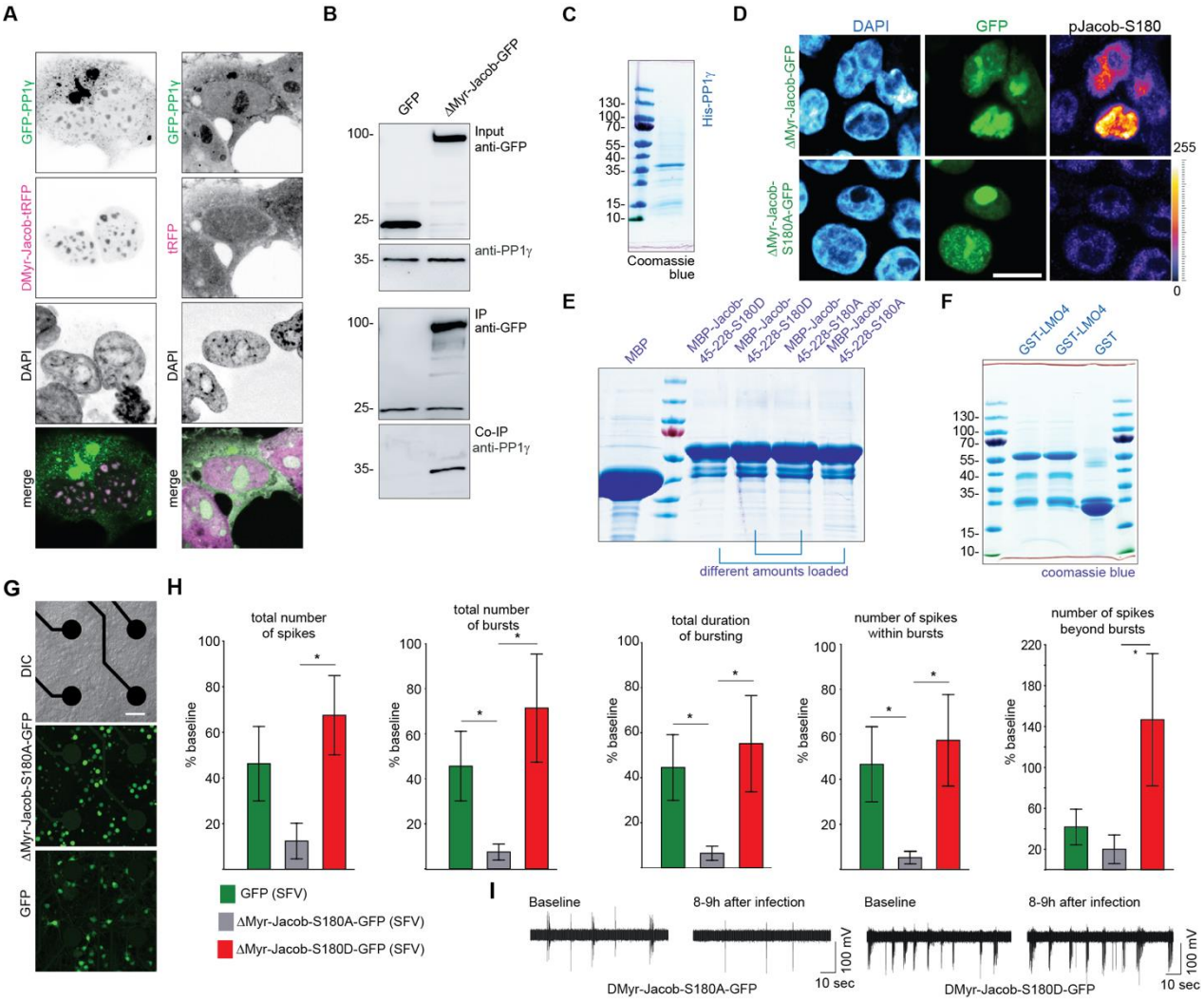

Fig. S3 (refers to Fig. 3) Confirmation of Jacob-PP1 interaction, protein purity and loading controls for pull down experiments and studies on the interaction and network activity depending on Jacob S180 phosphorylation.

(A) Confocal images of HEK293T cells overexpressing GFP-PP1γ together with ether ΔMyr-Jacob-tagRFP or tRFP control revealed nuclear co-clustering of both proteins. Scale bar: 20 µm.
(B) ΔMyr-Jacob-GFP but not GFP co-immunoprecipitate with endogenous PP1γ from HEK293T cells extracts.
(C) Coomassie blue stained gel showing purity of commercially available His-PP1γ.
(D) Nuclear Jacob (ΔMyr-Jacob-GFP), but not nuclear phosphodeficient mutant (ΔMyr-Jacob-S180A-GFP) expressed in HEK293T cells is phosphorylated. Confocal images of HEK293T cells overexpressing Jacob and immunostained with anti-pS180Jacob antibodies. Scale bar: 10 µm.
(E) Image of gels stained with coomassie blue showing the purity of bacterially produced Jacob mutants used for pull-down assay.
(F) Images of gels stained with coomassie blue showing inputs for bacterially produced GST-LMO4 coupled to beads used for pull-down assay with Jacob and PP1γ.
(G-I) Expression of phosphodeficient Jacob in the nucleus (ΔMyr-Jacob-S180A-GFP) strongly suppresses the spontaneous activity of neurons grown on microelectrode arrays (MEAs). **(G)** Representative images of infected hippocampal neurons. **(H)** Nuclear expression of phosphomimetic (ΔMyr-Jacob-S180D-GFP) or phosphodeficient (ΔMyr-Jacob-S180A-GFP) Jacob leads to significant enhancement or suppression of spontaneous neuronal activity, respectively. N=4 independent MEAs. *p<0.05 by Kruskal-Wallis ANOVA followed by multiple comparisons test. **(I)** Example traces of activity recorded immediately prior to and 8-9 h after viral infection.

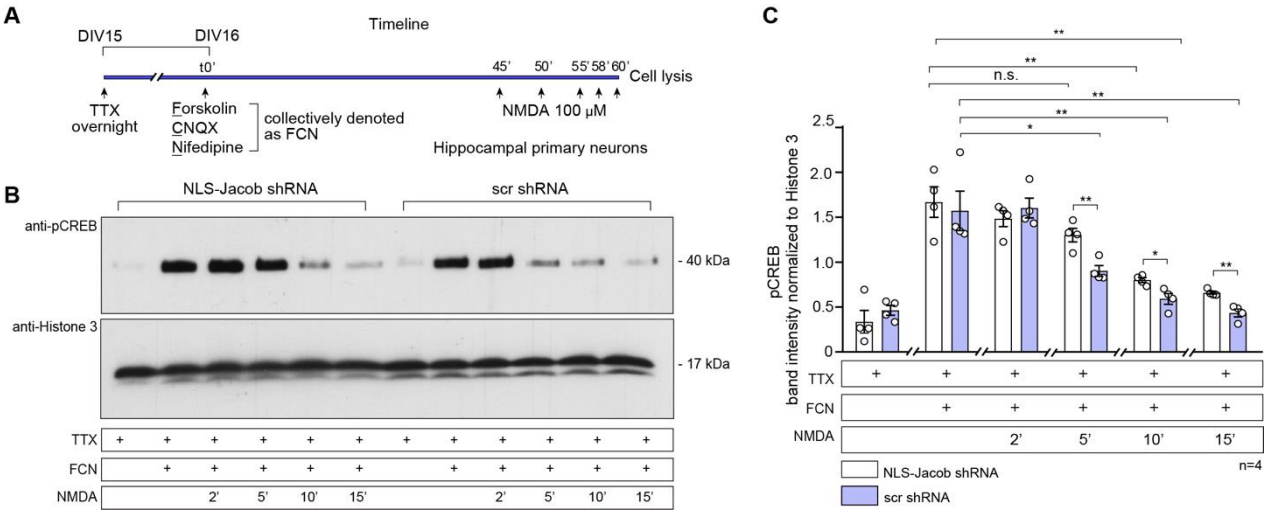

Fig. S4 Jacob knockdown partially rescues NMDAR-induced CREB shut-off

(A) Scheme representing the timeline of the experiment. Hippocampal cultures were silenced with TTX overnight and subsequently treated with forskolin, CNQX, and nifedipine. The time of NMDA bath application was 2, 5, 10 or 15 minutes.
(B) Representative immunoblot of total lysates probed with antibodies detecting pCREB and anti-Histone 3 as a loading control. Hippocampal neurons (DIV6) were infected with lentivirus carrying shRNA-NLS-GFP construct or scrambled control. At DIV15 neurons were treated as depicted in the scheme A.
(C) Nuclear Jacob knockdown partially rescues CREB shut-off after 5, 10 and 15 minutes of treatment with NMDA. Bar plot represents quantification of pCREB band intensity normalized to Histone 3. Data are represented as mean ± SEM. n=4 from independent

experiments. n.s.- non-significant where p>0,05, *p<0,05, **p<0,01 by two-tailed Student t-test.

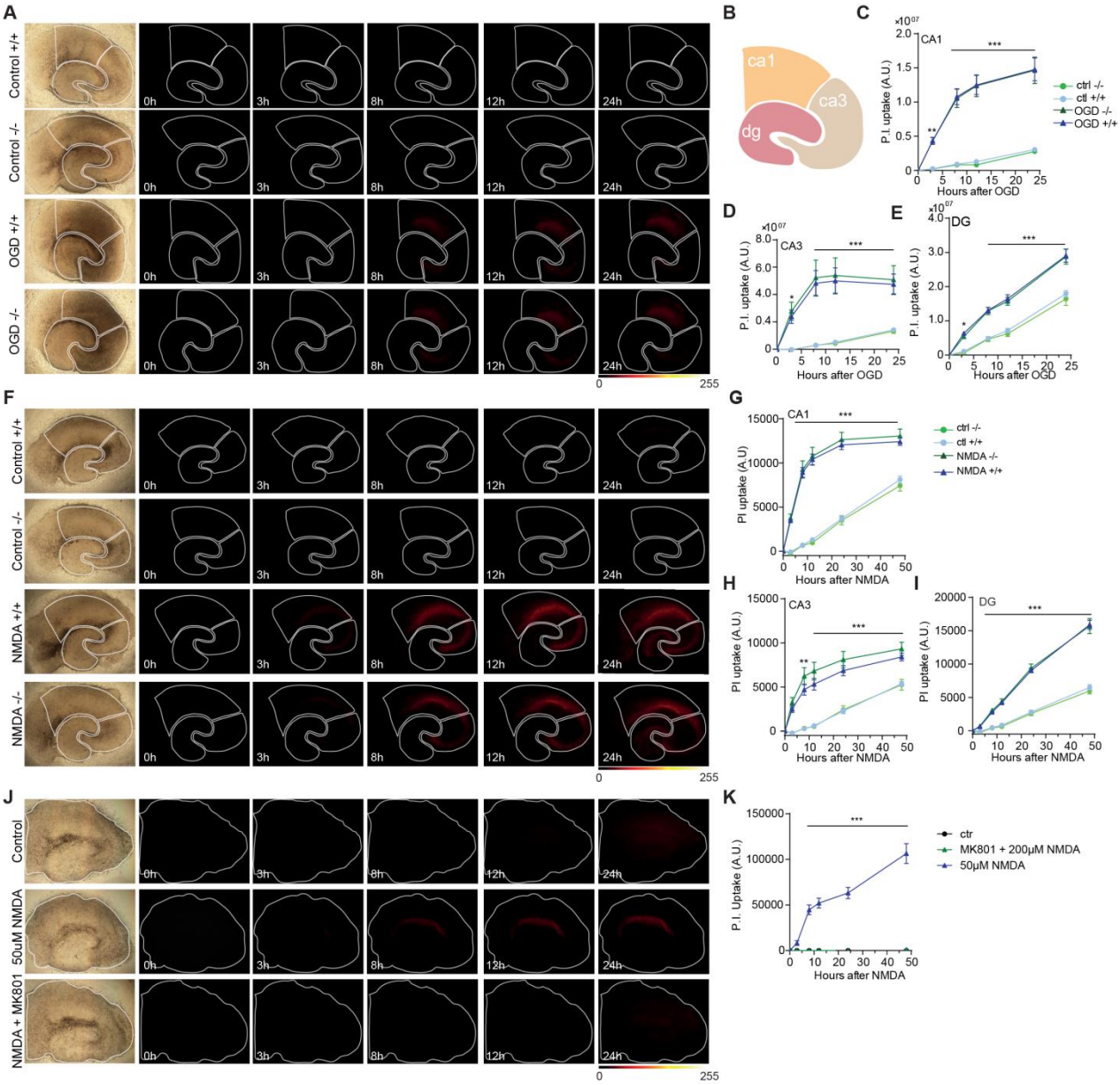

Fig. S5 Jacob gene knock-out does not influence the degree of OGD- and NMDA-induced cell death.

(A-E) Oxygen glucose deprivation (OGD) induced cell death in organotypic hippocampal slice culture irrespective of mice genotype.

(A) Fluorescent images of propidium iodide (PI) signal in organotypic hippocampal slices from wild type (+/+) and Jacob/*Nsmf* constitutive knock-out animals (-/-) after 0, 3, 8, 12, and 24h after 30 min OGD.

(B) Scheme representing CA1, CA3, and DG areas.

(C-E) Graphs representing the degree of PI uptake (A.U.) over time (h) after OGD insult. The OGD protocol induced cell death to the same degree in CA1(C), CA3 (D), and DG (E) irrespective of genotype. N=7-13 slices per group. **p<0,01, ***p<0,001 vs. control by RM-2way ANOVA followed by Bonferroni's multiple comparisons test. Data represented as mean ± SEM.

(F-I) Acute NMDA (50 μM) treatment induces the cell death in organotypic hippocampal slice culture irrespective of genotype.

(F) PI signal in organotypic hippocampal slices from wild type (+/+) animals after 0, 3, 8, 12, and 24h post treatment with 50 µM NMDA.
(G, H, I) Graphs representing the degree of PI uptake (A.U.) over time (h) after treatment with 50 µM NMDA. The 50 µM NMDA induced cell death to the same degree in CA1, CA3, and DG irrespective of genotype. N=6-15 slices per group. **p<0,01, ***p<0,001 vs. control by repeated measure two-way ANOVA followed by Bonferroni's multiple comparisons test. Data represented as mean ± SEM.
(J-K) MK801 blocks NMDA-induced cell death in organotypic slice culture irrespective of mice genotype. **(J)** PI signal in organotypic hippocampal slices from wild type (+/+) animals after 3, 8, 12, 24, and 48h after treatment with 50 µM NMDA. **(K)** The co-application of MK-801 completely abolished the effects of NMDA treatment. N=4-8 slices per group. ***p<0,001 vs. control by repeated measure two-way ANOVA followed by Bonferroni's multiple comparisons test. Data represented as mean ± SEM. Lookup table indicates the pixel intensities from 0 to 255.

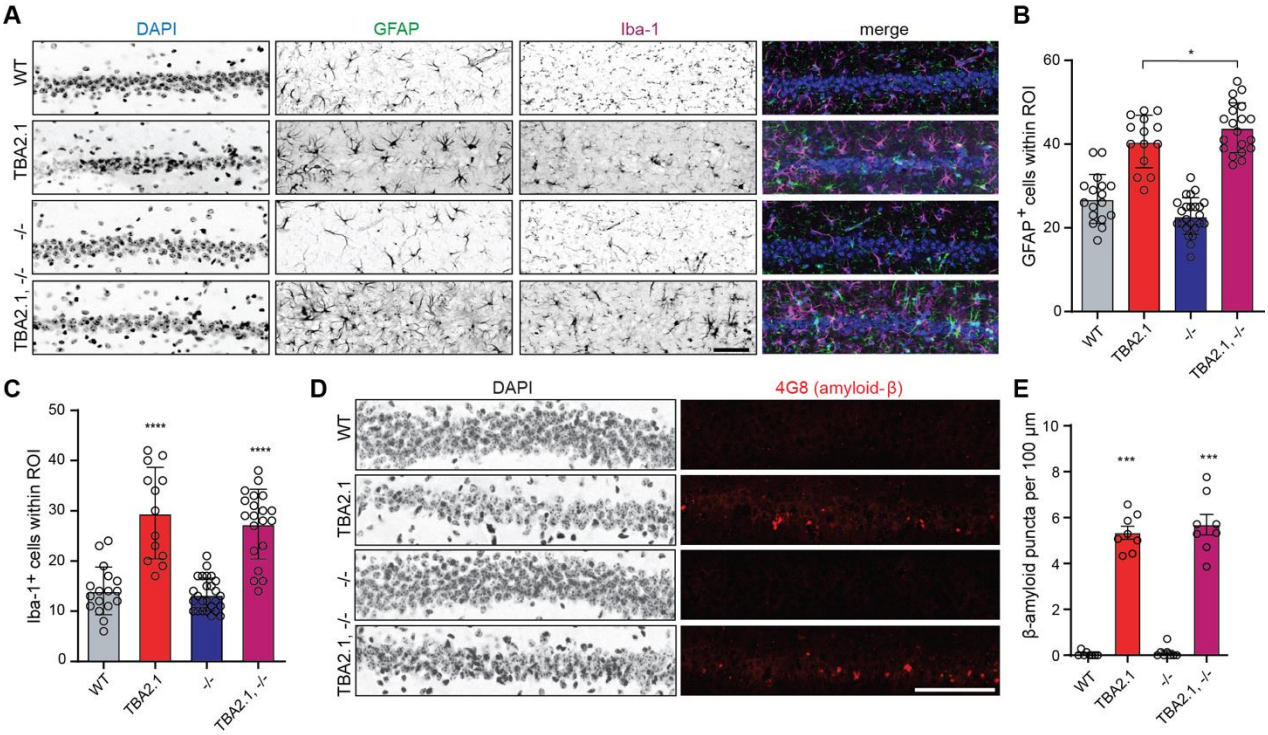

Fig. S6 Jacob/Nsmf deletion does not impact increased number of activated microglia, astrocytes and prominent deposition of amyloid-β in plaques.

(A) Representative confocal images of distal CA1 sections from 12 weeks old mice stained for GFAP, DAPI and Iba-1. Scale bar: 100 µm.
(B) Bar plot representing the number of GFAP positive cells per rectangular region of interest. N=17-24 cryosections from 5-7 animals per genotype. ****p<0,0001, *p<0,05 by two-way ANOVA with Bonferroni post hoc test. Data are represented as mean ± SEM.
(C) Bar plot representing the number of Iba-1 positive cells per rectangular region of interest. N=17-26 cryosections from 5-7 animals per genotype. ****p<0,0001 by two-way ANOVA with Bonferroni post hoc test. Data are represented as mean ± SEM.
(D) Confocal images averaged from two sections of the molecular layer of 12 weeks old mice distal CA1 labelled for amyloid-β (4G8 antibody) and co-stained with DAPI. Scale bar: 100 µm.
(E) Bar plot representing the number of amyloid-β positive puncta per 100 µm. N=8, number of cryosections from 2 animals per genotype. ***p<0,001 by two-way ANOVA with Bonferroni post hoc test. Data are represented as mean ± SEM.

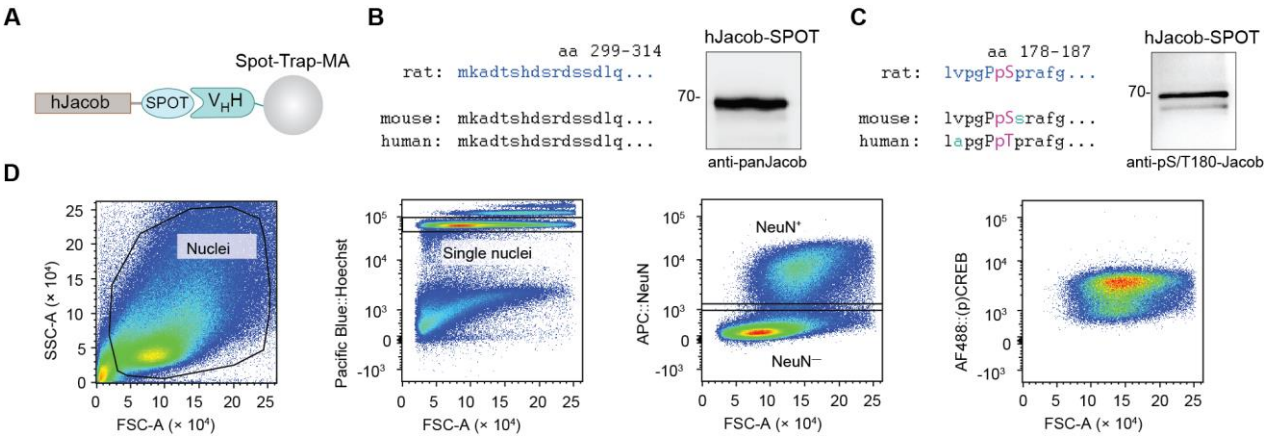

Fig. S7 (refers to Fig. 6) Anti-panJacob and anti-pJacob antibodies generated against rat peptide detect the human protein. The gating strategy for FACS.

(A) Schematic represents the immunoprecipitation approach employing Spot-nano Trap coupled to magnetic agarose (Chromotek) used for the enrichment of hJacob expressed in HEK293T cells for antibody detection.
(B) Rat amino acid sequence of Jacob used for generation of pan-Jacob antibodies is conserved throughout the species and the antibody effectively detects human Jacob.
(C) Despite variability within the peptide amino acid sequence used for the production of polyclonal pJacob antibodies they do recognize the human protein.
(D) Scatter plots representing gating strategy used in FACS experiments for neuronal pCREB and CREB immunoreactivity quantification.